

---

# DeepReShape: Redesigning Neural Networks for Efficient Private Inference

---

**Nandan Kumar Jha**  
 New York University  
 nj2049@nyu.edu

**Brandon Reagen**  
 New York University  
 bjr5@nyu.edu

## Abstract

Prior work on Private Inference (PI)—inferences performed directly on encrypted input—has focused on minimizing a network’s ReLUs, which have been assumed to dominate PI latency rather than FLOPs. Recent work has shown that FLOPs for PI can no longer be ignored, and also have high latency penalties. In this paper we develop DeepReShape: a network redesign technique that tailors architectures to PI constraints, optimizing for both ReLUs and FLOPs for the first time. The key insight is that a strategic allocation of channels such that the network’s ReLUs are distributed in their criticality order simultaneously optimizes both ReLU and FLOPs efficiency. DeepReShape automates network development with an efficient process, and we call generated networks HybReNets. We evaluate DeepReShape using standard PI benchmarks and demonstrate a 2.1% accuracy gain with a 5.2 $\times$  runtime improvement at iso-ReLU on CIFAR-100, and a 8.7 $\times$  runtime improvement at iso-accuracy on TinyImageNet. Finally, we show that prior PI-specific network optimizations are complimentary, and apply them to HybReNets for further benefit.

## 1 Introduction

As machine learning inferences are increasingly performed in the cloud, privacy concerns have emerged, resulting in the development of private inference (PI) where a client sends encrypted input to the cloud service provider, enabling inferences without exposing their data. While effective, the usage of complex cryptographic primitives [1–7] in PI results into substantially higher computational and storage overheads [8–13].

Prior work on PI-specific network optimization [14–21] has primarily focused on mitigating overheads associated with non-linear (ReLU) operations, assuming FLOPs are free. Specifically, methods such as CryptoNAS [14] and Sphynx [19] use neural architecture search to optimize ReLU efficiency and disregard FLOP implications. However, a recent work [13] has challenged this assumption, emphasizing that FLOPs do carry significant latency penalties.

Improving PI efficiency is further constrained by the limitations associated with current ReLU-optimization techniques. Their effectiveness largely depends on the selection of the input network, resulting in significant performance disparities that cannot be solely attributed to the FLOP count or accuracy of the input networks. Moreover, techniques such as DeepReDuce [17] encounter scalability issues and require considerable manual effort. While fine-grained ReLU optimization [20, 21] shows potential, its effectiveness is *confined* to networks with specific ReLU distributions and tends to *underperform* in networks with higher ReLU counts or altered ReLU distribution.

Another major challenge that persists in this domain is identifying network attributes that enhance PI performance. Current ReLU optimization methods [17, 20, 21] offer limited insight into the network features contributing to the improved PI performance. Moreover, it remains elusive whether a network with specific features can consistently outperform across various ReLU counts or if targeted ReLU counts determine the desired network attributes.

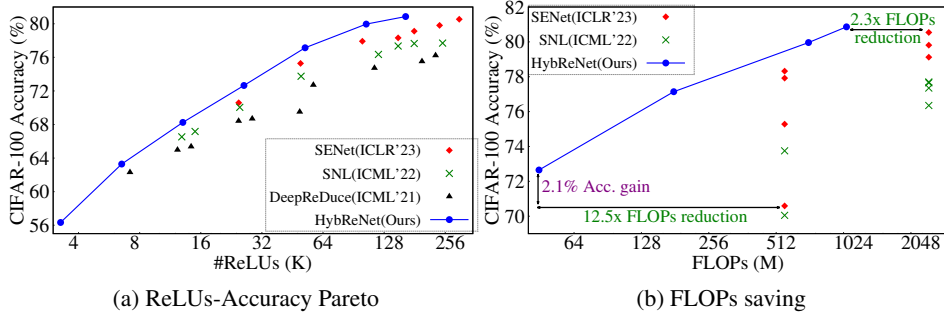


Figure 1: HybReNet outperforms state-of-the-art (SOTA) ReLU-optimization methods [21, 20, 17], achieving higher accuracy (CIFAR-100) and significant reduction in FLOPs while using fewer ReLUs.

Addressing these issues, we introduce a novel design principle, “ReLU-equalization,” which utilizes our main *insight* is that by expanding the network’s width while distributing its ReLUs according to their criticality order, we can control the FLOPs growth in deeper layers without sacrificing ReLU efficiency. Thus, achieving ReLU and FLOPs efficiency simultaneously.

Our *key observation*, termed “Capacity-Criticality-Tradeoff,” demonstrate that different network features are desirable for superior performance at varying ReLU counts. We find that wider networks are beneficial only for higher ReLU counts, while the proportion of non-critical ReLUs is crucial for lower ReLU counts. This observation *challenges the commonly held belief* that a network’s overall ReLU count is the key determinant for superior performance at lower ReLU counts. By utilizing this, we achieved a significant reduction, up to **45 $\times$** , in FLOPs when targeting lower ReLU counts.

Leveraging the above insights, we develop “DeepReShape,” to redesign the classical networks and synthesize PI-efficient networks “HybReNet” with a computational complexity of  $\mathcal{O}(1)$ . Our approach results in a substantial FLOPs reduction with fewer ReLUs, outperforming the state-of-the-art in PI. Specifically, compare to SENet [21], we achieve a  $2.3\times$  ReLU and  $3.4\times$  FLOPs reduction at iso-accuracy, and a  $2.1\%$  accuracy gain with a  $12.5\times$  FLOPs reduction at iso-ReLU on CIFAR-100. On TinyImageNet our approach saves  $12.4\times$  FLOPs at iso-accuracy.

Our key contributions are summarized as follows.

1. Perform an exhaustive characterization to understand the essential network characteristics, architecture and ReLUs’ distribution, for PI efficiency and demonstrate their generalizability.
2. Propose *ReLU-equalization*, a novel design principle for distributing the network’s ReLU in their criticality order, and designed a family of networks, *HybReNet*, tailored to the PI constraints.
3. Propose *ReLU-reuse*, a channel-wise ReLU dropping technique to systematically reduce the networks ReLUs count up to **16 $\times$** .

## 2 Preliminary

**Private inference protocols and threat model:** We use Delphi [9] protocols, as also used in [17, 20], for private inference. In particular, for linear layers Delphi performs compute-heavy homomorphic operations [1–3] in the offline phase (preprocessing) and additive secret sharing [22] in the online phase, once the client’s input is available. Whereas, for nonlinear(ReLU) layers it uses garbled circuits [23, 24]. Further, similar to, [25, 8, 9] we assume an honest-but-curious adversary where parties follow the protocols and learn nothing beyond their output shares.

**Architectural building blocks:** Figure 2 illustrates a schematic view of a standard four-stage network, with design hyperparameters. Similar to ResNet [26], it has a stem cell (to increase the channel count from 3 to  $m$ ), followed by the network’s main body (composed of linear and nonlinear layers, performing most of the computation), followed by a head (a fully connected layer) yielding the scores for the output classes. The network’s main body is composed of a sequence of four stages, and the spatial dimensions of feature maps ( $d_k \times d_k$ ) are progressively reduced by  $2\times$  in each stage (except Stage1), and feature dimensions remain constant within a stage. We keep the structure of the stem cell and head fixed and change the structure of the network’s body using design hyperparameters.

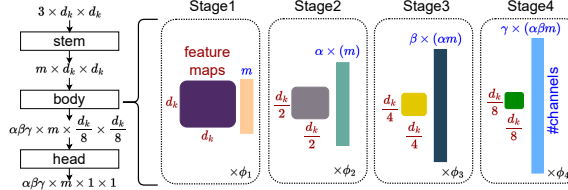


Figure 2: Depiction of architectural hyperparameters and feature dimensions in a four stage network. For ResNet18  $m = 64$ ,  $\phi_1 = \phi_2 = \phi_3 = \phi_4 = 2$ , and  $\alpha = \beta = \gamma = 2$ .  $\phi$  is the spatial size of kernel (e.g.,  $3 \times 3$ ).

Table 1: Network’s complexity (FLOPs and Params) per unit of nonlinearity varies with network’s width, and independent of the network’s depth. *Wider network require fewer ReLUs for a given complexity.* ( $f \times f$  ResNet18  $m = 64$ ,  $\phi_1 = \phi_2 = \phi_3 = \phi_4 = 2$ , and  $\alpha = \beta = \gamma = 2$ )

**Definitions and design hyperparameters:** Each stage is composed of identical blocks<sup>1</sup> repeated  $\phi_1$ ,  $\phi_2$ ,  $\phi_3$ , and  $\phi_4$  times in Stage1, Stage2, Stage3, and Stage4 (respectively), and known as *stage compute ratios*. The output channels in stem cell ( $m$ ) is known as *base channels*, and the number of channels progressively increases by a factor of  $\alpha$ ,  $\beta$ , and  $\gamma$  in Stage2, Stage3, and Stage4 (respectively), and we termed it as *stagewise channel multiplication factors*. These width and depth hyperparameters primarily determine the distribution of FLOPs, ReLUs, and parameters in the network. When we widen the network: (1) by augmenting  $m$ , which increases the #channels in each layer by the same factor, we denote this network as **BaseCh** (e.g., from  $m=64$  to  $m=128$ ); and (2) by homogeneously augmenting the  $(\alpha, \beta, \gamma)$ , we denote this network as **StageCh** (e.g., from  $(\alpha, \beta, \gamma) = (2, 2, 2)$  to  $(\alpha, \beta, \gamma) = (3, 3, 3)$ ).

### 3 Essential Network Attributes for Efficient Private Inference

We presents our key observations highlighting the influence of network architecture and their ReLUs’ distribution on the efficacy of private inference.

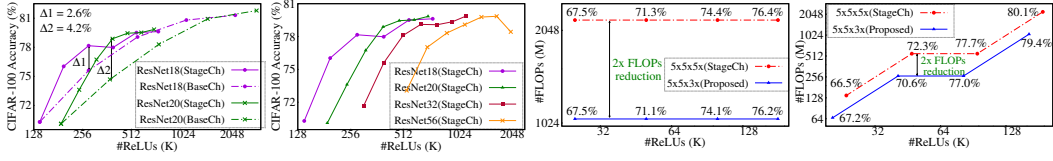
**Observation 1: ReLU’s criticality-aware network widening approach can address the FLOPs-ReLU-Accuracy imbalance, a key shortcoming of existing network widening methods.** Despite a line of seminal work on the network’s width expansion [27–30], the approaches to leverage the potential benefits of increased width without incurring FLOPs-ReLU-Accuracy imbalance remains elusive. The prevailing network widening method (BaseCh), including WideResNet [27], offers *limited* ReLU-efficiency due to the conservative  $(\alpha, \beta, \gamma) = (2, 2, 2)$  values<sup>2</sup>, which constrain channel growth in subsequent stages and restrict the network’s complexity per ReLU unit (see Table 1). Since prior ReLU optimization methods rely on classical networks, this limitation *prevents* the full realization of potential benefits associated with increased network width.

In contrast, StageCh networks significantly improve ReLU efficiency compared to BaseCh networks by removing the constraint on  $(\alpha, \beta, \gamma)$  and requiring fewer ReLUs for a given complexity (Figure 3(a)). However, the superiority of StageCh networks remains evident until reaching accuracy saturation, which varies with network configuration. In particular, as shown in Figure 3(b), accuracy saturation for StageCh networks of ResNet18, ResNet20, ResNet32, and ResNet56 models begins at  $(\alpha, \beta, \gamma) = (4, 4, 4)$ ,  $(5, 5, 5)$ ,  $(5, 5, 5)$ , and  $(6, 6, 6)$ , respectively, suggesting deeper StageCh network plateau at higher  $(\alpha, \beta, \gamma)$  values, and accurate prediction of saturation is challenging. This observations challenge the assertion made in [14], that model capacity per ReLU peaks at  $(\alpha, \beta, \gamma) = (4, 4, 4)$ . Consequently, *the extent to which a network can benefit from increased width for superior ReLU efficiency remains an open question*.

Our proposed ReLUs’ criticality-aware network widening approach effectively optimizes both ReLU and FLOPs efficiency, which a StageCh network fails to achieve as distinct homogeneous sets of  $(\alpha, \beta, \gamma)$  are required for FLOPs and ReLU efficiency. We leverage the *insight* that ReLU efficient StageCh networks suffer from rapidly increasing FLOPs in deeper layers, while our approach limits excessive FLOPs in deeper layers without compromising ReLU efficiency. Consequently, our approach attains ReLU efficiency on par with StageCh networks while significantly lowering FLOPs. For instance, Figure 3(c,d) demonstrates that the ReLUs’ criticality-aware ResNet18 network  $5 \times 5 \times 3$  maintains similar ReLU efficiency with a  $2 \times$  reduction in FLOPs count compared to the StageCh network  $5 \times 5 \times 5$ . This FLOPs reduction is consistently attained across the entire spectrum of ReLU counts, employing both fine-grained and coarse-grained ReLU optimization.

<sup>1</sup>Except the first block (in all but Stage1) which performs downsampling of feature maps by  $2 \times$ .

<sup>2</sup>Even the state-of-the-art vision model RegNets [31] have  $1.5 \leq (\alpha, \beta, \gamma) \leq 3$ , for FLOPs-efficiency reason.

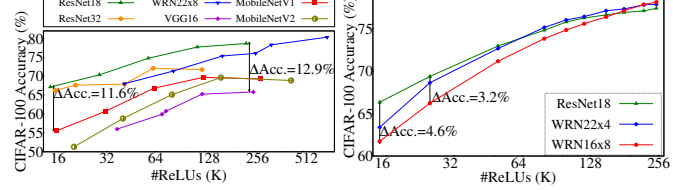


(a) StageCh vs BaseCh (b) Accuracy saturation (c) FLOPs saving w/ SNL (d) FLOPs saving w/ DRD  
Figure 3: (a) ReLU efficiency comparison for existing network widening methods (on ResNet): BaseCh and StageCh; (b) Accuracy saturation observed in StageCh. (c,d) 2 $\times$  FLOP reduction is achieved, while maintaining ReLU efficiency, for ReLUs’ criticality-aware 5x5x3x network with SNL and DeepReDuce ReLU optimization. Refer Appendix H for width hyperparameter settings.

**Observation2: Performance of ReLU optimization methods is strongly correlated with the choice of input networks, leading to substantial performance disparities.** Table 2 lists input networks used in previous ReLU optimization methods with their relevant characteristics, while Figure 4 demonstrates how different input networks impact DeepReDuce [17] and SNL [20]. For DeepReDuce, accuracy differences of **12.9%** and **11.6%** at higher and lower iso-ReLU counts are observed. *These differences cannot be ascribed to the FLOPs or accuracy of the baseline network alone.* For instance, ResNet18 outperforms WideResNet22x8 despite having 4.4 $\times$  fewer FLOPs and a lower baseline accuracy, and ResNet32 outperforms VGG16 even though the latter has 4.76 $\times$  more FLOPs and a higher baseline accuracy.

ReLU optimization method	Input networks			
Delphi [9]	ResNet32			
SAFEENets [15]	ResNet32, VGG16			
DeepReDuce [17]	ResNet18			
SNL [20] and SENet [21]	ResNet18, WRN22x8	WRN22x8	VGG16	MobileNetV1
	ResNet32	ResNet18	WRN22x8	MobileNetV2
FLOPs	70M	559M	246M	33.3M
ReLUs	303K	557K	1393K	285K
Acc	71.67%	79.06%	81.27%	75.08%

Table 2: Networks used in prior PI-specific ReLU optimization for advancing ReLU-Accuracy for advancing ReLU-Accuracy Pareto frontier (CIFAR-100).



(a) DeepReDuce [17] at iso-ReLU (b) SNL [20] at iso-ReLU  
Figure 4: Performance of ReLU optimization varies with the input networks, leading to a significant performance disparities.

Likewise, fine-grained ReLU optimization (SNL) exhibits significant accuracy differences when employed on ResNets and WideResNets, especially at lower ReLU counts as shown in Figure 4(b). While WideResNet models outperform beyond 200K ReLUs, there are 3.2% and 4.6% accuracy gaps at 25K and 15K ReLUs between ResNet18 and WideResNet16x8. A prevalent misconception is that a network with a lower ReLU count utilizes its ReLUs more efficiently, resulting in superior performance at lower ReLU counts. However, we demonstrate in Appendix C.3, that despite having fewer ReLUs than WideResNet models, the key driving factor for ResNet18’s enhanced performance is the proportion of the network’s ReLU in Stage1, rather than the total ReLU count.

**Observation 3: Distinct network attributes are required for superior PI efficiency at higher and lower ReLU counts (Capacity-Criticality-Tradeoff).** To examine the essential network characteristics for PI efficiency across a broad spectrum of ReLU counts, we select three iso-ReLU ResNet18 variants with distinct ReLUs’ distribution and FLOPs counts, achieved by altering the channel allocation per stage, in Table 3. In particular, 2x2x2x( $m=32$ ), 4x4x4x( $m=16$ ), and 3x7x2x( $m=16$ ) have stagewise channel allocation as [32, 64, 128, 256], [16, 64, 256, 1024], and [16, 48, 336, 672], respectively. We apply DeepReDuce and SNL on these networks and results are shown in Figure 5.

We observe that wider networks are superior *only* at higher ReLU counts while networks with a higher proportion of non-critical ReLUs excel at lower ReLU counts. This trend is consistent with both DeepReDuce and SNL. Specifically, wider models 4x4x4x( $m=16$ ) and 3x7x2x( $m=16$ ) outperform 2x2x2x( $m=32$ ) at higher ReLU counts; however, 2x2x2x( $m=32$ ) excel at lower ReLU counts despite having  $\approx 4\times$  fewer FLOPs. This performance is attributed to the higher fraction (58.82%) of non-critical Stage1 ReLUs in the 2x2x2x( $m=32$ ) model, as ReLU optimization methods primarily target these ReLUs when aiming for low counts. Consequently, networks with more Stage1 ReLUs need to eliminate fewer critical ReLUs, resulting in less accuracy degradation. For a thorough validation and explanation of the above observations, refer to Appendices C.2 and C.3.

The above findings offer insight into the accuracy trends for SNL in Figure 4(b), higher the Stage1 ReLU proportion (58.8% for ResNet18, 47.7% for WRN22x4, and 43.9% for WRN16x8) higher

Model	Acc(%)	FLOPs	ReLUs	Stagewise ReLUs' proportion			
				Stage1	Stage2	Stage3	Stage4
2x2x2x(m=32)	75.60	141M	279K	58.82%	23.53%	11.76%	5.88%
4x4x4x(m=16)	78.16	661M	279K	29.41%	23.53%	23.53%	23.53%
3x7x2x(m=16)	78.02	466M	260K	31.50%	18.90%	33.07%	16.54%

Table 3: A case study to investigate the capacity-criticality-tradeoff: Three Iso-ReLU ResNet18 models having distinct FLOPs count and ReLUs' distribution, achieved by altering channels allocation per stage(Stage1 ReLU count includes stem cell ReLUs).

the accuracy at lower ReLU counts. Moreover, it elucidates the rationale for choosing WRN22x8 (48.2% Stage1 ReLU proportion) for higher ReLU counts while ResNet18 for lower ReLU counts, for ReLU-accuracy Pareto in SNL and SENet [21].

**Observation 4: ReLU-Thinning improves the efficacy of fine-grained ReLU optimization, predominantly for networks possessing higher ReLU counts.** We employ a *hybrid* ReLU optimization approach and incorporate ReLU Thinning, a coarse-grained ReLU optimization step used in DeepReDuce, before SNL optimization. Interestingly, *even when baseline Thinned models are less accurate*, a significant boost (up to 3% at iso-ReLUs) in accuracy is observed, more pronounced for networks with higher #ReLUs (ResNet34 and WRN22x8, in Table 4). Since ReLU-Thinning drops the ReLUs from the network's alternate layers, *irrespective of their criticality*, its integration into existing ReLU optimization methodologies would not impact their overall computational complexity and remains effective for reducing the search space required to identify critical ReLUs.

	C100	Baseline	220K	180K	150K	120K	100K	80K	50K
ResNet18 (557.06K)	Vanilla	78.68	77.09	76.9	76.62	76.25	74.81	72.9	72.44
	w/ Th.	76.95	77.03	76.92	76.54	76.59	75.85	75.72	74.44
	$\Delta$	-1.73	-0.06	0.02	-0.34	0.07	0.91	1.48	
ResNet34 (966.66K)	Vanilla	79.67	76.55	76.35	76.26	75.47	74.55	74.17	72.07
	w/ Th.	79.03	77.94	77.65	77.67	75.32	76.69	76.32	74.50
	$\Delta$	-0.64	1.39	1.30	1.41	1.85	2.14	2.15	2.43
WRN22x8 (1392.64K)	Vanilla	80.58	77.58	76.83	76.15	74.98	74.38	73.16	71.13
	w/ Th.	79.59	78.91	78.6	78.41	78.05	77.22	75.94	72.74
	$\Delta$	-0.99	1.33	1.77	2.26	3.07	2.84	2.78	1.61

Table 4: A significant accuracy boost (on CIFAR-100) is achieved when ReLU-Thinning is employed prior to SNL, despite the less accurate ReLU-Thinned models.  $\Delta$  = Acc(w/ Th.)-Acc(Vanilla).

**Observation 5: Altering the network's ReLUs' distribution causes suboptimal performance in fine-grained ReLU optimization, and employing ReLU-Thinning reduces the performance gap.** We perform a contrastive analysis of fine-grained ReLU optimization (SNL) with DeepReDuce on the PI-amenable wider models 4x4x4x(m=16) and 3x7x2x(m=16), listed in Table 3. As shown in Figure 6(a) and 6(b) DeepReDuce outperforms SNL by a significant margin (upto 3%-4%); however, performing ReLU-Thinning before SNL optimization reduces this accuracy gap. This suggests that the benefit of fine-grained, over coarse-grained, ReLU optimization is *limited* to a specific ReLUs' distribution, and it diminishes in the network with a lower proportion of the network's ReLU in Stage1. This constraint applies to ReLU's criticality-aware networks as well, as shown in Figure 18.

## 4 DeepReShape

**Intuition for ReLUs' criticality-aware network widening:** We first examine the impact of existing network widening approaches (BaseCh and StageCh) on the network's ReLU distribution. Interestingly, we observe that increasing the network's width by augmenting  $\alpha$ ,  $\beta$ , and  $\gamma$  in StageCh networks results in a distinctive ReLU distribution, unlike BaseCh networks where all layers undergo the same scaling of #ReLUs. In particular, as illustrated in Figure 8, the proportion of Stage1 ReLUs decreases while that in other stages increases, and at higher  $(\alpha, \beta, \gamma)$ , where accuracy starts saturating, proportion in Stage4 dominates. This implies that the proportion of non-critical ReLUs is decreasing while the distribution of ReLUs among the other stages does not strictly adhere to their criticality order (see criticality evaluation in Table 8). This leads us to propose a network widening approach to increase the width until the ReLU distribution follows the criticality order, where *most-critical stage dominates the distribution*. We find that widening beyond the point where the network's ReLUs align with their criticality order does not significantly alter their relative distribution (Figure 8(c)).

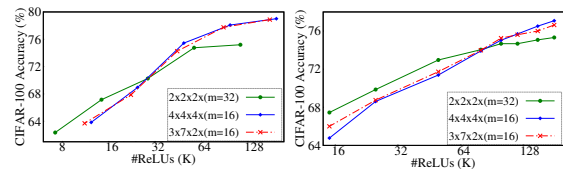


Figure 5: Capacity-Criticality-Tradeoff results: Figures (a) and (b) show the ReLU-Accuracy tradeoff for networks in Table 3 using DeepReDuce and SNL.

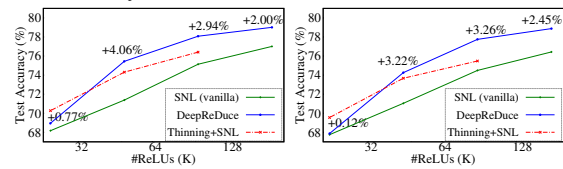


Figure 6: DeepReDuce outperforms SNL by a significant margin (up to 4%, CIFAR-100) when altering ReLU-Thinned networks reduces accuracy gap.

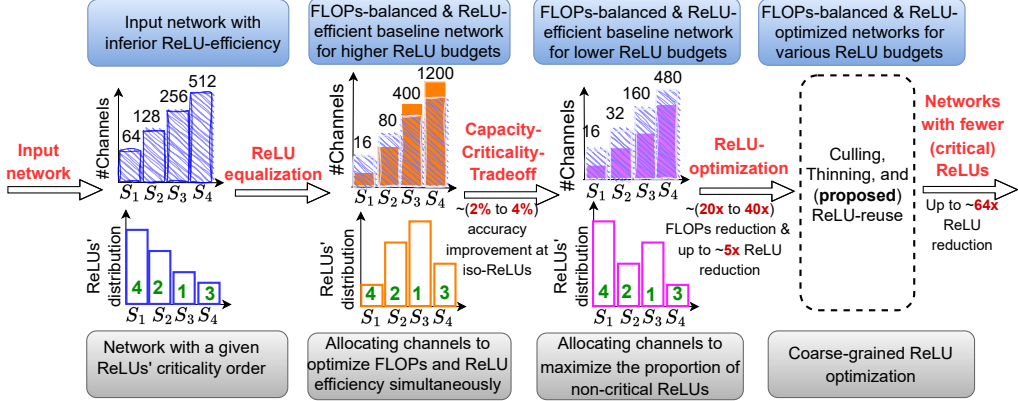


Figure 7: The DeepReShape network redesigning pipeline. ReLU’s criticality-aware strategic allocation of channels (gray boxes) outputs FLOPs-balanced ReLU-efficient baseline networks for various ReLU counts (blue boxes). Numbers in green denote criticality order (Stage3 is most critical).

**ReLU equalization and formation of HybReNet:** As illustrated in Figure 7, the ReLU-equalization step redistributes the network’s ReLU in their criticality order, i.e., the (most)least critical stage having a (highest)lowest fraction of the network’s ReLU. This is performed using an iterative process, as outlined in Algorithm 1, where in each iteration the relative distribution of ReLUs in two stages is rearranged in their criticality order, by altering network design hyperparameters. We select the sets of minimum values of  $(\alpha, \beta, \gamma)$  required for ReLU equalization and obtain four distinct HRN networks: HRN-5x5x3x, HRN-5x7x2x, HRN-6x6x2x, and HRN-7x5x2x (see Appendix A). Figure 7 shows the channel allocation, after ReLU-equalization, in the successive stages of HRN-5x5x3x, allocating fewer channels to initial stages more to deeper ones, compared to the input network.

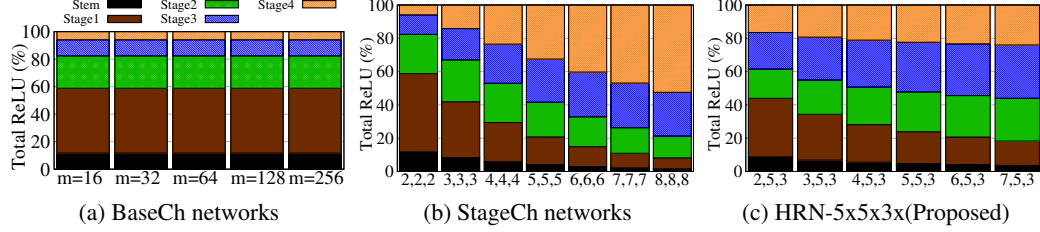


Figure 8: Impact of network’s width expansion on ReLU’s distribution: for ResNet18-based BaseCh (a), StageCh (b), and proposed HRN network (c). Once HRN network’s ReLU align in their criticality order (at 5,5,3), the relative distribution of ReLUs remains stable with increasing  $\alpha$  values.

**Network design for efficient PI at lower ReLU counts:** To enhance PI efficiency with lower ReLU counts, Stage1 needs to dominate the distribution of ReLUs (see observation 3); however, ReLU equalization in HRNs led to the lowest proportion of network ReLUs in Stage1. To address this, the  $\alpha$  value in HRNs is reduced to 2 as the decreasing  $\alpha$  value results in an increased proportion of Stage1 ReLUs. Consequently, HRN-2x5x3x, HRN-2x5x2x, HRN-2x6x2x, and HRN-2x7x2x have Stage1 dominating the network’s ReLUs’ distribution (see Table 9), and distribution of ReLUs in all but Stage1 follow their criticality order. Figure 7 shows the channel reallocation in HRN-2x5x3x after considering Capacity-Criticality-Tradeoff, allocating fewer channels even in deeper stages which results in significant FLOPs, up to  $\sim 45\times$  reduction.

### ReLU-reuse (Re2):

We propose *ReLU-reuse*, to drop the ReLUs selectively from all but a (contiguous)fraction of feature maps in a layer. Inspired by [32, 33], feature maps of the layer are divided into  $N$  groups and ReLUs are employed only to the last group (Figure 9). Empirically, increasing the value of  $N$  results in a significant accuracy loss, despite  $1 \times 1$  convolution being employed for cross-channel interaction. This is likely due to the loss of cross-channel information arises from a greater number of divisions in the feature

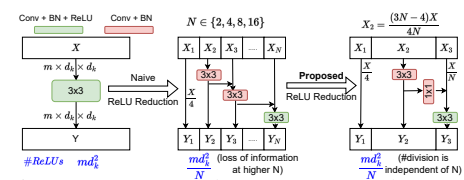


Figure 9: Proposed ReLU-reuse where ReLUs are selectively used in a fraction of channels, reducing network’s ReLUs up to  $16\times$ .

maps (see our ablation study in Table 14, Appendix G). To address this issue, we devise a mechanism that decouples the number of divisions in feature maps from the ReLU reduction factor  $N$ . Precisely, one-fourth of channels are utilized for feature reuse, while a  $N$ th fraction of feature maps are activated using ReLUs, and the remaining feature maps are processed solely with convolution operations, resulting in only three groups. It is important to note that using the ReLUs in the last group of feature maps increases the effective receptive field as those neurons can take into account a greater portion of the input feature maps, using the skip connections.

## 5 Experimental Results

**Analysis of HybReNets Pareto points:** Figure 1 shows that HybReNet advances the ReLU-accuracy Pareto with a substantial reduction in FLOPs counts – a factor overlooked in prior PI-specific network optimization. Now, we present a detailed analysis of network configurations and ReLU optimization steps and quantify their benefits for ReLUs and FLOPs reduction. We use ResNet18-based HRN-5x5x3x for ReLU-accuracy comparison with SOTA PI methods in Figure 1, as its FLOPs efficiency is superior to other HRNs (see Table 16).

Table 5: Network configurations and ReLU optimization steps used for the Pareto points in Figure 1, on CIFAR-100. Re2 denotes ReLU-reuse, used for achieving very low ReLU-counts.

HybReNet	$m$	ReLU optimization steps			#ReLU	#FLOPs	Accuracy(%)		Acc./ReLU
		Culled	Thinned	Re2			KD[34]	DKD[35]	
5x5x3x	16	NA	S1+S2+S3+S4	NA	163.3K	1055.4M	79.34	80.86	0.50
2x5x3x	32	S1	S2+S3+S4	NA	104.4K	714.1M	77.63	79.96	0.77
2x5x3x	16	S1	S2+S3+S4	NA	52.2K	178.5M	74.98	77.14	1.48
2x5x3x	8	S1	S2+S3+S4	NA	26.1K	44.6M	70.36	72.65	2.78
2x5x3x	16	S1	S2+S3+S4	4	13.1K	121.6M	67.30	68.25	5.23
2x5x3x	16	S1	S2+S3+S4	8	6.5K	130.5M	62.68	63.29	9.70
2x5x3x	16	S1	S2+S3+S4	16	3.2K	137.2M	56.24	56.33	17.26

The key takeaway from Table 5 is that tailoring the network features for PI constraint significantly reduces FLOPs along with ReLUs. Specifically, lowering  $\alpha$  value and base channel count led to  $23.6 \times$  fewer FLOPs in HRN-2x5x3x( $m=8$ ), compared to HRN-5x5x3x( $m=16$ ). Moreover, the criticality-aware ReLUs’ distribution in HRNs simplifies the complexity of ReLU optimization steps to  $\mathcal{O}(1)$ , as opposed to the iterative steps in DeepReDuce that lead to  $\mathcal{O}(D)$  complexity for a  $D$  stage network. In particular, we apply ReLU Culling only to Stage1 if it dominates the network ReLU distribution, such as HRNs with  $\alpha=2$ , and employ ReLU-Thinning for the remaining stages. Further reduction in ReLU count is achieved by implementing ReLU-reuse with a suitable reduction factor, as shown in Table 5. Finally, an accuracy boost is achieved by employing DKD [35], as the ReLU-reduced models greatly benefit from decoupling the target and non-target class distillation.

Note that we exclusively employ coarse-grained ReLU optimization steps for HRNs, based on the observation that fine-grained ReLU optimization techniques underperform when the distribution of ReLU is altered in classical networks (see Figure 6). Therefore, fine-grained ReLU optimization fails to take advantage of increased network complexity per ReLU unit in HRNs and remains subpar compared to classical networks. For an in-depth discussion, see Appendix C.4.

**HybReNets outperform state-of-the-art in private inference:** Table 6 presents competing design points for SENet [21] and SNL [20], and we select HybReNet points offering both accuracy and latency benefits for a fair comparison. The runtime breakdown is presented as homomorphic (HE) latency [1–3], arises from linear operations (convolution and fully-connected layers), and Garbled-circuit (GC) latency [36, 36, 24], resulting from non-linear (ReLU) operations [9, 10, 13].

On CIFAR-100, SENet requires 300K ReLUs and 2461M FLOPs to reach 80.54% accuracy; whereas, HRN-5x5x3x achieves 80.86% accuracy with only 163K ReLUs and 1055M FLOPs, providing  $1.8 \times$  ReLU and  $2.3 \times$  FLOPs saving. Similarly, at 25K ReLUs, our approach achieves a 2.1% accuracy gain with  $12.5 \times$  FLOPs reduction, thereby saving  $5.2 \times$  runtime. Even at an extremely low ReLU count of 13K, HRN is 1.7% more accurate and achieves  $2.2 \times$  runtime saving, compared to the SNL.

On TinyImageNet, HybReNets outperform SENet at both 300K and 142K ReLUs, improve runtime by  $1.7 \times$  and  $8.7 \times$ , respectively. Compared to SNL at 489K ReLUs, HybReNets are 3.2% (1.7%) more accurate with a  $1.8 \times$  ( $2.8 \times$ ) reduction in runtime. At lower ReLU counts of 100K and 59K,

Table 6: Comparison of HybReNet with state-of-the-art in private inference: SENet [21] and SNL [20]. HybReNet exhibits superior ReLU and FLOPs efficiency and achieve a substantial reduction in latency. #Re and #FL denote ReLU and FLOPs counts; Acc. is top-1 accuracy; Lat. is the runtime for one private inference, including Homomorphic (HE) and Garbled-circuit(GC) latencies.

	SOTA in Private Inference						HybReNet(Ours)						Improvements					
	#Re	#FL	Acc.	HE	GC	Lat.	#Re	#FL	Acc.	HE	GC	Lat.	#Re	#FL	Acc.	HE	GC	Lat.
CIFAR-100 [21]	300	2461	80.54	1004	33.7	1037	163	1055	80.86	770	18.4	788	1.8 $\times$	2.3 $\times$	0.3	1.3 $\times$	1.8 $\times$	1.3 $\times$
	240	2461	79.81	1004	27.0	1031	163	1055	80.86	770	18.4	788	1.5 $\times$	2.3 $\times$	1.1	1.3 $\times$	1.5 $\times$	1.3 $\times$
	180	2461	79.12	1004	20.2	1024	163	1055	80.86	770	18.4	788	1.1 $\times$	2.3 $\times$	1.7	1.3 $\times$	1.1 $\times$	1.3 $\times$
	50	559	75.28	268	5.6	274	52	179	77.14	123	5.9	129	1.0 $\times$	3.1 $\times$	1.9	2.2 $\times$	0.9 $\times$	2.1 $\times$
	25	559	70.59	268	2.8	271	26	45	72.65	49	2.9	52	0.9 $\times$	12.5 $\times$	2.1	5.5 $\times$	1.0 $\times$	5.2 $\times$
TinyImageNet [21]	15	559	67.17	268	1.7	270	13	179	68.25	123	1.5	124	1.1 $\times$	3.1 $\times$	1.1	2.2 $\times$	1.1 $\times$	2.2 $\times$
	13	559	66.53	268	1.5	270	13	179	68.25	123	1.5	124	1.0 $\times$	3.1 $\times$	1.7	2.2 $\times$	1.0 $\times$	2.2 $\times$
	300	2227	64.96	927	33.7	961	327	1055	64.92	526	36.7	563	0.9 $\times$	2.1 $\times$	0.0	1.8 $\times$	0.9 $\times$	1.7 $\times$
	142	2227	58.90	927	16.0	943	104	179	58.90	97	11.7	108	1.4 $\times$	12.4 $\times$	0.0	9.6 $\times$	1.4 $\times$	8.7 $\times$
	489	9830	64.42	3690	55.0	3745	653	4216	67.58	2029	73.4	2102	0.7 $\times$	2.3 $\times$	3.2	1.8 $\times$	0.7 $\times$	1.8 $\times$
[20]	489	9830	64.42	3690	55.0	3745	418	2842	66.10	1307	45.0	1352	1.2 $\times$	3.5 $\times$	1.7	2.8 $\times$	1.2 $\times$	2.8 $\times$
	298	2227	64.04	927	33.5	961	327	1055	64.92	526	36.7	563	0.9 $\times$	2.1 $\times$	0.9	1.8 $\times$	0.9 $\times$	1.7 $\times$
	100	2227	58.94	927	11.2	939	104	179	58.90	97	11.7	108	1.0 $\times$	12.4 $\times$	0.0	9.6 $\times$	1.0 $\times$	8.7 $\times$
	59	2227	54.40	927	6.6	934	52	712	54.46	329	5.9	335	1.1 $\times$	3.1 $\times$	0.1	2.8 $\times$	1.1 $\times$	2.8 $\times$

HybReNets match the accuracy with SNL and achieve a  $12.4\times$  and  $3.1\times$  FLOPs reduction, which results in  $8.7\times$  and  $2.8\times$  runtime improvement, respectively.

Our primary insight from Table 6 is that FLOPs reduction does not inherently guarantee a proportional reduction in HE latency, whereas a direct correlation exists between ReLU reduction and GC latency savings. In particular, a  $\sim 12.5\times$  FLOPs reduction translates to  $5.2\times$  and  $8.7\times$  latency reduction on CIFAR-100 and TinyImageNet, respectively. This is due to the fact HE latency has an intricate dependency on the input/output packing [8, 37], rotational complexity [38–40] and slot utilization [41]. We refer the readers to [8, 10] for details.

**Generality case study on ResNet34:** We select ResNet34 for DeepReShape generality study for two key reasons: (1) its consistent use for the case study in prior PI-specific network optimization studies [17, 20, 21], and (2) its stage compute ratio ( $\phi_1=3$ ,  $\phi_2=4$ ,  $\phi_3=6$ , and  $\phi_4=3$ ) distinguishes it from ResNet18, results in different sets of HRN networks, HRN-4x6x3x and HRN-4x9x2x, upon applying Algorithm 1. We use HRN-4x6x3x for comparison with SOTA in Table 7.

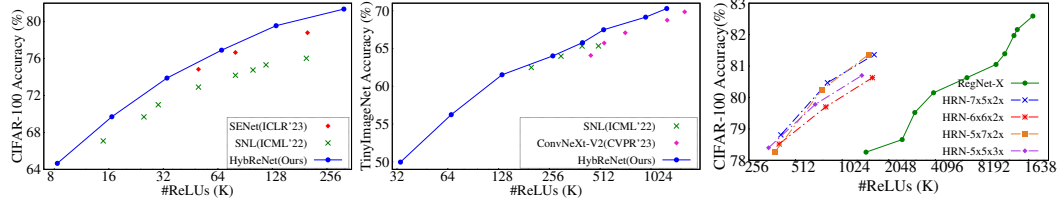


Figure 10: HybReNet models surpass the SOTA ReLU-optimization methods [21, 20] applied to ResNet34. Moreover, they outperform SOTA vision models RegNets[31] and ConvNeXt-V2 [42].

HybReNet advances the ReLU-accuracy Pareto on both CIFAR-100 and TinyImageNet, shown in Figures 10 (a, b). Table 7 quantifies the FLOPs-ReLU-Accuracy benefits along with runtime savings. On CIFAR-100, compared to SOTA, HybReNet improves runtime by  $3.1\times$  with a significant gain in accuracy — 9.8%, 7.2%, 5.9%, and 2.1% at 15K, 25K, 30K and 50K ReLUs (respectively). Further on TinyImageNet, SNL requires 300K ReLUs and 4646M FLOPs to reach 64% accuracy; whereas, HybReNet matches this accuracy with  $8.8\times$  fewer FLOPs, leading to a runtime improvement of  $6.3\times$ . Conclusively, it highlights the effectiveness of DeepReShape and validates its generality.

**HybRNets outperform SOTA vision models ConvNeXt and RegNet:** We select SOTA vision models ConvNeXt-V2 [42] and RegNet [31] for our comparative analysis with HybReNets as these models possess distinctive depth/width hyperparameters, compared to the ResNet (Appendix E.4).

First, we compare the baseline RegNet-X models with (ResNet18-based) HybReNets on CIFAR-100, without applying any ReLU-optimization steps. Results are shown in Figure 10(c) where HRNs are evaluated with  $m \in \{16, 32, 64\}$ . All HRNs achieve a substantial reduction in ReLU count, at iso-accuracies. For instance, to achieve accuracies of 78.26% and 80.63%, RegNet-X models

Table 7: ResNet34-based HybReNets outperform SOTA PI methods [21, 20] employed on ResNet34, and also surpass the current state-of-the-art vision models ConvNeXt-V2[42] . #Re and #FL denote ReLU and FLOPs counts; Acc. is top-1 accuracy; Lat. is the runtime for one private inference.

	#Re	#FL	SOTA in Private Inference (on ResNet34)					HybReNet(Ours)					Improvements					
			Acc.	HE	GC	Lat.	#Re	#FL	Acc.	HE	GC	Lat.	#Re	#FL	Acc.	HE	GC	Lat.
CIFAR-100	200	1162	78.80	459	22.5	482	134	527	79.56	404	15.1	419	1.5 $\times$	2.2 $\times$	0.8	1.1 $\times$	1.5 $\times$	1.1 $\times$
	80	1162	76.66	459	9.0	468	67	132	76.91	140	7.5	148	1.2 $\times$	8.8 $\times$	0.3	3.3 $\times$	1.2 $\times$	3.2 $\times$
	50	1162	74.84	459	5.6	465	67	132	76.91	140	7.5	148	0.7 $\times$	8.8 $\times$	2.1	3.3 $\times$	0.7 $\times$	3.1 $\times$
	30	1162	71.00	459	3.4	462	67	132	76.91	140	7.5	148	0.4 $\times$	8.8 $\times$	<b>5.9</b>	3.3 $\times$	0.4 $\times$	<b>3.1<math>\times</math></b>
	25	1162	69.68	459	2.8	462	67	132	76.91	140	7.5	148	0.4 $\times$	8.8 $\times$	<b>7.2</b>	3.3 $\times$	0.4 $\times$	<b>3.1<math>\times</math></b>
	15	1162	67.08	459	1.7	461	67	132	76.91	140	7.5	148	0.2 $\times$	8.8 $\times$	<b>9.8</b>	3.3 $\times$	0.2 $\times$	<b>3.1<math>\times</math></b>
TinyImageNet	500	4646	65.34	1710	56.2	1766	537	2109	67.48	880	60.3	940	0.9 $\times$	2.2 $\times$	2.1	1.9 $\times$	0.9 $\times$	2.3 $\times$
	400	4646	65.32	1710	45.0	1755	537	2109	67.48	880	60.3	940	0.7 $\times$	2.2 $\times$	2.2	1.9 $\times$	0.7 $\times$	2.3 $\times$
	300	4646	63.99	1710	33.7	1744	268	529	64.02	245	30.2	275	1.1 $\times$	8.8 $\times$	0.0	7.0 $\times$	1.1 $\times$	<b>6.3<math>\times</math></b>
	200	4646	62.49	1710	22.5	1733	268	529	64.02	245	30.2	275	0.7 $\times$	8.8 $\times$	1.5	7.0 $\times$	0.7 $\times$	<b>6.3<math>\times</math></b>
	1622	11801	69.85	4067	182.4	4249	1270	8244	70.29	3091	142.8	3233	1.3 $\times$	1.4 $\times$	0.4	1.3 $\times$	1.3 $\times$	1.3 $\times$
	1278	9080	68.75	2368	143.7	2512	952	4638	69.15	1837	107.1	1944	1.3 $\times$	2.0 $\times$	0.4	1.3 $\times$	1.3 $\times$	1.3 $\times$
ConvNeXt	721	3436	67.08	1307	81.0	1388	537	2109	67.48	880	60.3	940	1.3 $\times$	1.6 $\times$	0.4	1.5 $\times$	1.3 $\times$	1.5 $\times$
	541	1935	65.72	738	60.8	799	402	1187	65.77	592	45.2	637	1.3 $\times$	1.6 $\times$	0.0	1.3 $\times$	1.3 $\times$	1.3 $\times$
	451	1345	64.07	546	50.7	597	268	529	64.02	245	30.2	275	1.7 $\times$	2.5 $\times$	0.0	2.2 $\times$	1.7 $\times$	2.2 $\times$

require 1460K and 6544K ReLUs respectively, while the HRN-5x5x3x only requires 343K and 1372K ReLUs, leading to a  $4.3\times$  and  $4.7\times$  ReLU reduction respectively.

Now, we compare the ConvNeXt-V2 models with HybReNets on TinyImageNet, after employing ReLU optimization steps. The ReLU-accuracy Pareto is shown in Figure 10(b), with a detailed comparison outlined in Table 7. The competing HRNs achieve  $1.3\times$  to  $1.7\times$  ReLU savings;  $1.4\times$  to  $2.5\times$  FLOPs reduction; which results in  $1.3\times$  to  $2.3\times$  runtime improvements.

**Sensitivity study and analysis of networks produced by DeepReShape:** We analyze the impact of each stagewise channel multiplication factor ( $\alpha, \beta, \gamma$ ) on the network’s ReLU and FLOPs efficiency using a sensitivity analysis. With ResNet18 configured with  $m=16$ , we systematically vary one factor at a time, starting from 2, while other factors are held constant at 2.

We observe that augmenting  $\alpha$  and  $\beta$  values improves ReLU efficiency; notably, the latter optimizes the performance marginally better than the former until a saturation point is reached. On the other hand, FLOPs efficiency is most effectively improved by augmenting  $\alpha$ , outperforming  $\beta$  enhancements while augmenting  $\gamma$  values yields the worst FLOPs-efficiency. This suggests that FLOPs growth in the deeper layers of StageCh networks is inconsequential. Conclusively, higher  $\alpha$  and  $\beta$  values with a *restrictive*  $\gamma$  value are desirable for FLOPs-ReLU-Accuracy balance.

We find that ReLU equalization in HRNs confines the  $\gamma$  values (see Appendix A). Precisely, all the four HRNs produced by DeepReShape method; HRN-5x5x3x, HRN-5x7x2x, HRN-6x6x2x, and HRN-7x5x2x; posses higher  $\alpha$  and  $\beta$  values while  $\gamma$  values are restricted as  $\gamma < 4$ . Thus, higher  $\alpha$  and  $\beta$  values in HRNs boost ReLU efficiency, and a lower  $\gamma$  value restricts the FLOPs’ growth in deeper layers, promoting FLOP efficiency.

## 6 Related Work

**PI-specific network optimization:** Delphi [9] and SAFENet [15] substitute the ReLUs with low-degree polynomials, while DeepReDuce [17] is a coarse-grained ReLU optimization and drops ReLUs layerwise. SNL [20] and SENet [21] are fine-grained ReLU optimization, and drops the pixelwise ReLUs. CryptoNAS [14] and Sphynx [19] use neural architecture search and employ constant number of ReLUs per layer for designing ReLU-efficient networks, disregarding FLOPs implications. In contrast, our approach achieves ReLU and FLOPs efficiency simultaneously. We refer the reader to [43] for detailed HE and GC-specific optimizations for private inference, and Appendix I for additional related work.

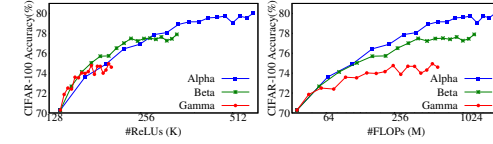


Figure 11: Sensitivity analysis for ReLUs and FLOPs efficiency (ResNet18 on CIFAR-100).

## 7 Conclusion

In this work, we develop the DeepReShape method to achieve ReLU and FLOPs efficiency simultaneously and designed a novel family of networks named HybReNet. We further study the essential network attributes enabling PI efficiency over a wide range of ReLU counts. Our findings demonstrate that distinct network attributes are required for efficient PI at higher and lower ReLU counts.

## 8 Checklist

**Broader impact:** The privacy-preserving computations often necessitates significant resources, such as memory and compute time. For instance, the use of the garbled-circuit technique alone requires hundreds of gigabytes of memory, and homomorphic computations can take hours for a single private inference. This demand for resources highlights the necessity for efficient optimization strategies. Previously, a line of research on specialized hardware architectures and protocol optimizations have been put forward to address these overheads. However, these approaches come with their own limitations: the former presents sustainability issues [44], and the latter can introduce new security vulnerabilities and lack backward compatibility.

Contrastingly, algorithmic enhancements can be effectively deployed across a variety of hardware platforms and security protocols. In our research, we demonstrate that a substantial reduction in runtime,  $\sim(5\times \text{ to } 10\times)$ , can be achieved simply by strategically allocating channels in existing classical networks and employing straightforward ReLU optimization steps. Importantly, this decrease does not depend on specific network architectures or specialized hardware, thus broadening the potential impact of our algorithmic optimization work.

**Limitations:** Achieving a specific ReLU count with HRNs is challenging due to the use of coarse-grained ReLU optimization steps, which are influenced by the base channel counts and stage-wise channel multiplication factors. The difference between fine-grained and coarse-grained ReLU optimization lies in their performance and configurability to a target ReLU count. Fine-grained ReLU optimization allows for an independent target ReLU count input, while coarse-grained ReLU optimization adjusts based on the network’s ReLU count. However, when applied to HRNs, fine-grained ReLU optimization has been found to underperform compared to the coarse-grained approach.

**Reproducibility statements:** We have provided all the implementation-specific details in Appendix H. Further, the details of the network architecture can be found in Appendix J. Also, the details of the ReLU optimization steps are presented in Table 5, Table 11, and Table 12.

## Acknowledgment

We would like to thank Karthik Garimella for his assistance in computing the runtime (HE and GC latency) for private inference. This research was developed with funding from the Defense Advanced Research Projects Agency (DARPA), under the Data Protection in Virtual Environments (DPRIVE) program, contract HR0011-21-9-0003. The views, opinions and/or findings expressed are those of the author and should not be interpreted as representing the official views or policies of the Department of Defense or the U.S. Government.

## References

- [1] Craig Gentry et al. *A fully homomorphic encryption scheme*. 2009.
- [2] Junfeng Fan and Frederik Vercauteren. *Somewhat practical fully homomorphic encryption*. *Cryptology ePrint Archive*, 2012.
- [3] Zvika Brakerski, Craig Gentry, and Vinod Vaikuntanathan. *(leveled) fully homomorphic encryption without bootstrapping*. *ACM Transactions on Computation Theory*, 2014.
- [4] Jung Hee Cheon, Andrey Kim, Miran Kim, and Yongsoo Song. *Homomorphic encryption for arithmetic of approximate numbers*. In *International conference on the theory and application of cryptology and information security*, 2017.

- [5] Daniel Demmler, Thomas Schneider, and Michael Zohner. Aby-a framework for efficient mixed-protocol secure two-party computation. In *The Network and Distributed System Security Symposium*, 2015.
- [6] Payman Mohassel and Peter Rindal. Aby3: A mixed protocol framework for machine learning. In *Proceedings of the ACM SIGSAC Conference on Computer and Communications Security*, 2018.
- [7] Arpita Patra, Thomas Schneider, Ajith Suresh, and Hossein Yalame. Aby2.0: Improved mixed-protocol secure two-party computation. In *30th USENIX Security Symposium*, 2021.
- [8] Chiraag Juvekar, Vinod Vaikuntanathan, and Anantha Chandrakasan. Gazelle: A low latency framework for secure neural network inference. In *27th USENIX Security Symposium*, 2018.
- [9] Pratyush Mishra, Ryan Lehmkuhl, Akshayaram Srinivasan, Wenting Zheng, and Raluca Ada Popa. Delphi: A cryptographic inference service for neural networks. In *29th USENIX Security Symposium*, 2020.
- [10] Deevashwer Rathee, Mayank Rathee, Nishant Kumar, Nishanth Chandran, Divya Gupta, Aseem Rastogi, and Rahul Sharma. Cryptflow2: Practical 2-party secure inference. In *Proceedings of the ACM SIGSAC Conference on Computer and Communications Security*, 2020.
- [11] Sijun Tan, Brian Knott, Yuan Tian, and David J Wu. Cryptgpu: Fast privacy-preserving machine learning on the gpu. In *IEEE Symposium on Security and Privacy*, 2021.
- [12] Yongqin Wang, G Edward Suh, Wenjie Xiong, Benjamin Lefaudoux, Brian Knott, Murali Annavaram, and Hsien-Hsin S Lee. Characterization of mpc-based private inference for transformer-based models. In *IEEE International Symposium on Performance Analysis of Systems and Software (ISPASS)*, 2022.
- [13] Karthik Garimella, Zahra Ghodsi, Nandan Kumar Jha, Siddharth Garg, and Brandon Reagen. Characterizing and optimizing end-to-end systems for private inference. In *Proceedings of the 28th ACM International Conference on Architectural Support for Programming Languages and Operating Systems*, 2023.
- [14] Zahra Ghodsi, Akshaj Kumar Veldanda, Brandon Reagen, and Siddharth Garg. CryptoNAS: Private inference on a relu budget. In *Advances in Neural Information Processing Systems*, 2020.
- [15] Qian Lou, Yilin Shen, Hongxia Jin, and Lei Jiang. SAFENet: Asecure, accurate and fast neu-ral network inference. *International Conference on Learning Representations*, 2021.
- [16] Karthik Garimella, Nandan Kumar Jha, and Brandon Reagen. Sisyphus: A cautionary tale of using low-degree polynomial activations in privacy-preserving deep learning. In *ACM CCS Workshop on Private-preserving Machine Learning*, 2021.
- [17] Nandan Kumar Jha, Zahra Ghodsi, Siddharth Garg, and Brandon Reagen. DeepReDuce: Relu reduction for fast private inference. In *International Conference on Machine Learning*, 2021.
- [18] Zahra Ghodsi, Nandan Kumar Jha, Brandon Reagen, and Siddharth Garg. Circa: Stochastic relus for private deep learning. In *Advances in Neural Information Processing Systems*, 2021.
- [19] Minsu Cho, Zahra Ghodsi, Brandon Reagen, Siddharth Garg, and Chinmay Hegde. Sphynx: Relu-efficient network design for private inference. *IEEE Security & Privacy*, 2022.
- [20] Minsu Cho, Ameya Joshi, Siddharth Garg, Brandon Reagen, and Chinmay Hegde. Selective network linearization for efficient private inference. In *International Conference on Machine Learning*, 2022.
- [21] Souvik Kundu, Shunlin Lu, Yuke Zhang, Jacqueline Liu, and Peter A Beerel. Learning to linearize deep neural networks for secure and efficient private inference. In *The Eleventh International Conference on Learning Representations*, 2023.
- [22] Adi Shamir. How to share a secret. *Communications of the ACM*, 1979.

[23] Andrew Chi-Chih Yao. How to generate and exchange secrets. In *27th Annual Symposium on Foundations of Computer Science*, 1986.

[24] Marshall Ball, Brent Carmer, Tal Malkin, Mike Rosulek, and Nichole Schimanski. Garbled neural networks are practical. *Cryptology ePrint Archive*, 2019.

[25] Jian Liu, Mika Juuti, Yao Lu, and N Asokan. Oblivious neural network predictions via minionn transformations. In *Proceedings of the ACM SIGSAC Conference on Computer and Communications Security*, 2017.

[26] Kaiming He, Xiangyu Zhang, Shaoqing Ren, and Jian Sun. Deep residual learning for image recognition. In *Proceedings of the IEEE conference on computer vision and pattern recognition*, 2016.

[27] Sergey Zagoruyko and Nikos Komodakis. Wide residual networks. *arXiv preprint*, 2016.

[28] Ilija Radosavovic, Justin Johnson, Saining Xie, Wan-Yen Lo, and Piotr Dollár. On network design spaces for visual recognition. In *Proceedings of the IEEE/CVF international conference on computer vision*, 2019.

[29] Jaehoon Lee, Lechao Xiao, Samuel Schoenholz, Yasaman Bahri, Roman Novak, Jascha Sohl-Dickstein, and Jeffrey Pennington. Wide neural networks of any depth evolve as linear models under gradient descent. *Advances in neural information processing systems*, 32, 2019.

[30] Piotr Dollár, Mannat Singh, and Ross Girshick. Fast and accurate model scaling. In *Proceedings of the IEEE/CVF Conference on Computer Vision and Pattern Recognition*, 2021.

[31] Ilija Radosavovic, Raj Prateek Kosaraju, Ross Girshick, Kaiming He, and Piotr Dollár. Designing network design spaces. In *Proceedings of the IEEE/CVF Conference on Computer Vision and Pattern Recognition*, 2020.

[32] Shanghua Gao, Ming-Ming Cheng, Kai Zhao, Xin-Yu Zhang, Ming-Hsuan Yang, and Philip HS Torr. Res2net: A new multi-scale backbone architecture. In *IEEE transactions on pattern analysis and machine intelligence*, 2019.

[33] Shihua Huang, Zhichao Lu, Kalyanmoy Deb, and Vishnu Naresh Boddeti. Revisiting residual networks for adversarial robustness: An architectural perspective. In *Proceedings of the IEEE/CVF Conference on Computer Vision and Pattern Recognition*, 2023.

[34] Geoffrey Hinton, Oriol Vinyals, and Jeff Dean. Distilling the knowledge in a neural network. *arXiv preprint arXiv:1503.02531*, 2015.

[35] Borui Zhao, Quan Cui, Renjie Song, Yiyu Qiu, and Jiajun Liang. Decoupled knowledge distillation. In *Proceedings of the IEEE/CVF Conference on computer vision and pattern recognition*, 2022.

[36] Vladimir Kolesnikov, Payman Mohassel, and Mike Rosulek. Flexor: Flexible garbling for xor gates that beats free-xor. In *Annual Cryptology Conference*, 2014.

[37] Ehud Aharoni, Alon Adir, Moran Baruch, Nir Drucker, Gilad Ezov, Ariel Farkash, Lev Greenberg, Ramy Masalha, Guy Moshkowich, Dov Murik, et al. Helyers: A tile tensors framework for large neural networks on encrypted data. *Proceedings on privacy enhancing technologies*, 2023.

[38] Qian Lou, Wen-jie Lu, Cheng Hong, and Lei Jiang. Falcon: fast spectral inference on encrypted data. *Advances in Neural Information Processing Systems*, 2020.

[39] Qian Lou, Song Bian, and Lei Jiang. Autoprivacy: Automated layer-wise parameter selection for secure neural network inference. In *Advances in Neural Information Processing Systems*, pages 8638–8647, 2020.

[40] Zhicong Huang, Wen jie Lu, Cheng Hong, and Jiansheng Ding. Cheetah: Lean and fast secure Two-Party deep neural network inference. In *31st USENIX Security Symposium*, 2022.

[41] Eunsang Lee, Joon-Woo Lee, Junghyun Lee, Young-Sik Kim, Yongjune Kim, Jong-Seon No, and Woosuk Choi. Low-complexity deep convolutional neural networks on fully homomorphic encryption using multiplexed parallel convolutions. In *International Conference on Machine Learning*, 2022.

[42] Sanghyun Woo, Shoubhik Debnath, Ronghang Hu, Xinlei Chen, Zhuang Liu, In So Kweon, and Saining Xie. Convnext v2: Co-designing and scaling convnets with masked autoencoders. In *Proceedings of the IEEE/CVF Conference on Computer Vision and Pattern Recognition*, 2023.

[43] Lucien KL Ng and Sherman SM Chow. Sok: Cryptographic neural-network computation. In *2023 IEEE Symposium on Security and Privacy (SP)*, 2023.

[44] Udit Gupta, Mariam Elgamal, Gage Hills, Gu-Yeon Wei, Hsien-Hsin S Lee, David Brooks, and Carole-Jean Wu. Act: Designing sustainable computer systems with an architectural carbon modeling tool. In *Proceedings of the 49th Annual International Symposium on Computer Architecture*, pages 784–799, 2022.

[45] Zhuang Liu, Hanzi Mao, Chao-Yuan Wu, Christoph Feichtenhofer, Trevor Darrell, and Saining Xie. A convnet for the 2020s. In *Proceedings of the IEEE/CVF Conference on Computer Vision and Pattern Recognition*, 2022.

[46] Jason Yosinski, Jeff Clune, Yoshua Bengio, and Hod Lipson. How transferable are features in deep neural networks? *Advances in neural information processing systems*, 27, 2014.

[47] Microsoft SEAL (release 4.0). <https://github.com/Microsoft/SEAL>, March 2022. Microsoft Research, Redmond, WA.

[48] Christian Szegedy, Vincent Vanhoucke, Sergey Ioffe, Jon Shlens, and Zbigniew Wojna. Rethinking the inception architecture for computer vision. In *Proceedings of the IEEE conference on computer vision and pattern recognition*, 2016.

[49] Mikhail Belkin, Daniel Hsu, Siyuan Ma, and Soumik Mandal. Reconciling modern machine-learning practice and the classical bias–variance trade-off. *Proceedings of the National Academy of Sciences*, 2019.

[50] Preetum Nakkiran, Gal Kaplun, Yamini Bansal, Tristan Yang, Boaz Barak, and Ilya Sutskever. Deep double descent: Where bigger models and more data hurt. *Journal of Statistical Mechanics: Theory and Experiment*, 2021.

[51] Gowthami Somepalli, Liam Fowl, Arpit Bansal, Ping Yeh-Chiang, Yehuda Dar, Richard Baraniuk, Micah Goldblum, and Tom Goldstein. Can neural nets learn the same model twice? investigating reproducibility and double descent from the decision boundary perspective. In *Proceedings of the IEEE/CVF Conference on Computer Vision and Pattern Recognition*, 2022.

[52] Saining Xie, Ross Girshick, Piotr Dollár, Zhuowen Tu, and Kaiming He. Aggregated residual transformations for deep neural networks. In *Proceedings of the IEEE conference on computer vision and pattern recognition*, 2017.

[53] Hanxiao Liu, Karen Simonyan, and Yiming Yang. Darts: Differentiable architecture search. *arXiv preprint*, 2018.

[54] Mingxing Tan and Quoc Le. Efficientnet: Rethinking model scaling for convolutional neural networks. In *International Conference on Machine Learning*, 2019.

[55] Andrew Howard, Mark Sandler, Grace Chu, Liang-Chieh Chen, Bo Chen, Mingxing Tan, Weijun Wang, Yukun Zhu, Ruoming Pang, Vijay Vasudevan, et al. Searching for mobilenetv3. In *Proceedings of the IEEE/CVF International Conference on Computer Vision*, 2019.

[56] Mingxing Tan, Bo Chen, Ruoming Pang, Vijay Vasudevan, Mark Sandler, Andrew Howard, and Quoc V Le. Mnasnet: Platform-aware neural architecture search for mobile. In *Proceedings of the IEEE Conference on Computer Vision and Pattern Recognition*, 2019.

[57] Alex Krizhevsky, Vinod Nair, and Geoffrey Hinton. Cifar-10 (canadian institute for advanced research). *URL* <http://www.cs.toronto.edu/kriz/cifar.html>, 2010.

- [58] Ya Le and Xuan Yang. Tiny imagenet visual recognition challenge. *CS 231N*, 7, 2015.
- [59] Leon Yao and John Miller. Tiny imagenet classification with convolutional neural networks. *CS 231N*, 2015.
- [60] Ilya Loshchilov and Frank Hutter. Sgdr: Stochastic gradient descent with warm restarts. *arXiv preprint arXiv:1608.03983*, 2016.
- [61] Seyed Iman Mirzadeh, Arslan Chaudhry, Dong Yin, Huiyi Hu, Razvan Pascanu, Dilan Gorur, and Mehrdad Farajtabar. Wide neural networks forget less catastrophically. In *International Conference on Machine Learning*, 2022.
- [62] Hao Li, Zheng Xu, Gavin Taylor, Christoph Studer, and Tom Goldstein. Visualizing the loss landscape of neural nets. *Advances in neural information processing systems*, 2018.
- [63] Anna Golubeva, Guy Gur-Ari, and Behnam Neyshabur. Are wider nets better given the same number of parameters? In *International Conference on Learning Representations*, 2021.
- [64] Thao Nguyen, Maithra Raghu, and Simon Kornblith. Do wide and deep networks learn the same things? uncovering how neural network representations vary with width and depth. In *International Conference on Learning Representations*, 2021.
- [65] Julie Chang, Vincent Sitzmann, Xiong Dun, Wolfgang Heidrich, and Gordon Wetzstein. Hybrid optical-electronic convolutional neural networks with optimized diffractive optics for image classification. *Scientific reports*, 2018.
- [66] Gordon HY Li, Ryoto Sekine, Rajveer Nehra, Robert M Gray, Luis Ledezma, Qiushi Guo, and Alireza Marandi. All-optical ultrafast relu function for energy-efficient nanophotonic deep learning. *Nanophotonics*, 2022.
- [67] Kai Y. Xiao, Vincent Tjeng, Nur Muhammad (Mahi) Shafiuallah, and Aleksander Madry. Training for faster adversarial robustness verification via inducing reLU stability. In *International Conference on Learning Representations*, 2019.
- [68] Mislav Balunović and Martin Vechev. Adversarial training and provable defenses: Bridging the gap. In *International Conference on Learning Representations*, 2020.
- [69] Tianlong Chen, Huan Zhang, Zhenyu Zhang, Shiyu Chang, Sijia Liu, Pin-Yu Chen, and Zhangyang Wang. Linearity grafting: Relaxed neuron pruning helps certifiable robustness. In *International Conference on Machine Learning*, 2022.
- [70] Daniel Franzen and Michael Wand. General nonlinearities in  $so(2)$ -equivariant cnns. In *Advances in Neural Information Processing Systems*, 2021.
- [71] Taco S. Cohen and Max Welling. Steerable CNNs. In *International Conference on Learning Representations*, 2017.
- [72] Maurice Weiler, Mario Geiger, Max Welling, Wouter Boomsma, and Taco S Cohen. 3d steerable cnns: Learning rotationally equivariant features in volumetric data. *Advances in Neural Information Processing Systems*, 2018.
- [73] Maurice Weiler and Gabriele Cesa. General  $e(2)$ -equivariant steerable cnns. *Advances in Neural Information Processing Systems*, 2019.

## A ReLU Equalization and Development of HybReNet Networks

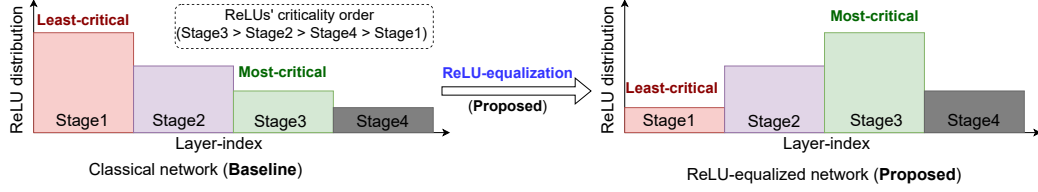


Figure 12: Schematic illustration of ReLU-equalization: Unlike conventional networks (e.g., ResNet) where ReLUs’ arrangement is *agnostic* to their significance, ReLU-equalization strategically redistributes ReLUs according to their criticality order.

---

### Algorithm 1 ReLU equalization

---

**Input:** Network  $Net$  with stages  $S_1, \dots, S_D$ ;  $C$  a sorted list of most to least critical stage; stage-compute ratio  $\phi_1, \dots, \phi_D$ ; and stagewise channel multiplication factors  $\lambda_1, \dots, \lambda_{(D-1)}$ .

**Output:** ReLU-equalized versions of network  $Net$ .

```

1: for  $i = 1$  to  $D-1$  do
2:    $S_k = C[i]$                                  $\triangleright C[1]$  is most critical stage
3:    $S_t = C[i+1]$                              $\triangleright C[2]$  is second-most critical stage
4:    $\#ReLUs(S_k) > \#ReLUs(S_t)$             $\triangleright$  Evaluate the compound inequality
5:    $\implies \frac{\phi_k \times \left( \prod_{j=1}^{k-1} \lambda_j \right)}{2^{k-1}} > \frac{\phi_t \times \left( \prod_{j=1}^{t-1} \lambda_j \right)}{2^{t-1}}$ 
6: end for
7: return A set of  $\phi_1, \dots, \phi_D$  and  $\lambda_1, \dots, \lambda_{(D-1)}$  satisfying above compound inequality.

```

---

Given a baseline classical network, ReLU equalization redistribute the network’s ReLU in their criticality order, i.e., the (most)least critical stage having (highest)lowest fraction of network’s total ReLU count (see Figure 12). This is performed using an iterative process, as outlined in Algorithm 1, where in each iteration the relative distribution of ReLUs in two stages is adjusted in their criticality order, by altering their design hyperparameters. Precisely, ReLU equalization on a  $D$  stage network with  $ChMulFacts$  as  $\lambda_1, \dots, \lambda_{(D-1)}$ , and stage compute ratio as  $\phi_1, \dots, \phi_D$  outputs a compound inequality, after  $D-1$  iterations. Finally, after solving the compound inequality, we get a set of width and depth hyperparameter values for ReLU equalized versions of baseline network. We employ Algorithm 1 on a standard four-stage network illustrated in Figure 2, with the criticality order arranged from the most critical to the least critical as  $S_3 > S_2 > S_4 > S_1$  (refer to Table 8). It outputs the following compound inequalities.

$$\#ReLUs(S_3) > \#ReLUs(S_2) > \#ReLUs(S_4) > \#ReLUs(S_1) \\ \implies \phi_3 \left( \frac{\alpha\beta}{16} \right) > \phi_2 \left( \frac{\alpha}{4} \right) > \phi_4 \left( \frac{\alpha\beta\gamma}{64} \right) > \phi_1$$

$$\text{ReLU equalization through depth } (\alpha = \beta = \gamma = 2) : \implies \frac{\phi_3}{4} > \frac{\phi_2}{2} > \frac{\phi_4}{8} > \phi_1$$

$$\text{ReLU equalization through width } (\phi_1 = \phi_2 = \phi_3 = \phi_4 = 2, \text{ and } \alpha \geq 2, \beta \geq 2, \gamma \geq 2) :$$

$$\implies \frac{\alpha\beta}{16} > \frac{\alpha}{4} > \frac{\alpha\beta\gamma}{64} > 1 \implies \alpha\beta > 16, \alpha > 4, \alpha\beta\gamma > 64, \beta > 4, \beta\gamma < 16, \text{ and } \gamma < 4$$

Solving the above compound inequalities provides the following  $(\beta, \gamma)$  pairs and the range of  $\alpha$ :

The  $(\beta, \gamma)$  pairs are:  $(5, 2)$  &  $\alpha \geq 7$ ;  $(5, 3)$  &  $\alpha \geq 5$ ;  $(6, 2)$  &  $\alpha \geq 6$ ;  $(7, 2)$  &  $\alpha \geq 5$

We obtain four pairs of  $(\beta, \gamma)$  along with an  $\alpha$  value range that satisfy the ReLU equalization requirements. Now to find the exact value of  $\alpha$ , we sweep the  $\alpha$  values, beginning from  $\alpha=2$ , and examine their impact on ReLUs’ distribution. We find that, similar to StageCh networks, the proportion of Stage1 ReLUs keep decreasing in HRNs until the network achieves ReLU equalization, at a specific value of  $\alpha$  (Figure 13). However, unlike StageCh networks, increasing  $\alpha$  beyond ReLU

equalization does not change the relative distribution of stagewise ReLUs. As a result, we get four baseline networks: HRN-7x5x2x, HRN-5x5x3x, HRN-6x6x2x, and HRN-5x7x2x whose  $\alpha$ s are the minimum value of  $\alpha$  enabling ReLU equalization with the given  $(\beta, \gamma)$  pairs (see Appendix A.2). The architectural details of these four HRNs are presented in Table 16.

### A.1 Computational Complexity of Designing HybReNet

For a  $D$  stage network with predetermined (stagewise)ReLUs’ criticality order, ReLU equalization typically requires the consideration of  $2D-1$  hyperparameters, comprising  $D$  stage compute ratio and  $D-1$  *ChMulFacts*. This hyperparameter count is reduced to  $D-1$  for HRN networks as the ReLU equalization is performed by altering network’s width alone. Finally, unlike the SoTA network designing methods [31, 45], hyperparameters are determined by solving a compound inequality and *do not necessitate additional network training*. Thus, the computational complexity of designing HRNs is characterized as  $\mathcal{O}(1)$ .

### A.2 Rationale Behind Choosing Specific $\alpha$ , $\beta$ , and $\gamma$ Values in HybReNet Networks

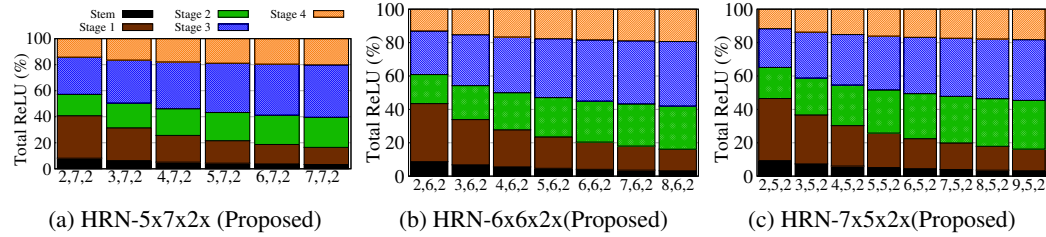


Figure 13: ReLU distribution analysis in HRN networks by progressively increasing the  $\alpha$  values from  $\alpha=2$ , enabling a comprehensive characterization of ReLU distribution. Once the network’s achieve ReLU equalization – (5, 7, 2) for HRN-5x7x2x, (6, 6, 2) for HRN-6x6x2x, and (7, 5, 2) for HRN-7x5x2x – the (relative) ReLU distribution remains stable with increasing  $\alpha$  value.

We chose the smallest  $\alpha$  values within a specified range for the given four pairs of  $(\beta, \gamma)$  based on two main considerations. Firstly, when the network attains ReLU equalization, the ReLU distribution becomes stable and stays constant as  $\alpha$  grows. This stability stems from fact that altering  $\alpha$  has the least impact on the relative distribution of stage-wise ReLUs compared to increasing  $\beta$  and  $\gamma$ . Specifically, increasing  $\alpha$  results in a slight decrease in the proportion of Stage1 and a slight increase in the proportion of the remaining stages. Secondly, when ReLU optimization (DeepReLUce) is employed, increasing alpha in HRNs does not improve the ReLU efficiency. Instead, it results in a inferior ReLU-accuracy tradeoff at lower ReLU counts, as shown in Figure 14.

## B Effects of Network Width and ReLUs’ Distribution on the Criticality Order of ReLUs

Table 8: Evaluating Stagewise ReLU Criticality in ResNet18 (R18) *BaseCh* and *StageCh* Networks, on CIFAR-100. The criticality metric values ( $C_k$ ) for each stage are determined using the [17] method. *Notably, the criticality order for both BaseCh and StageCh networks remains identical to the original ResNet18 sequence:  $S_3 > S_2 > S_4 > S_1$  (Higher  $C_k$  implies more critical ReLUs)*

Networks	Stage1			Stage2			Stage3			Stage4		
	#ReLUs	Acc(%)	+KD(%)	$C_k$	#ReLUs	Acc(%)	+KD(%)	$C_k$	#ReLUs	Acc(%)	+KD(%)	$C_k$
R18(m=16)-2x2x2x	81.92K	52.08	52.67	0.00	32.77K	61.24	62.10	7.39	16.38K	63.00	64.64	9.84
R18(m=32)-2x2x2x	163.84K	59.19	60.19	0.00	65.54K	65.91	66.47	4.69	32.77K	65.7	67.28	5.55
R18(m=64)-2x2x2x	327.68K	62.65	63.13	0.00	131.07K	67.18	68.32	3.69	65.54K	68.75	70.29	5.34
R18(m=128)-2x2x2x	655.36K	62.34	64.15	0.00	262.14K	69.28	70.56	4.34	131.07K	71.25	72.04	5.61
R18(m=256)-2x2x2x	1310.72K	64.81	65.22	0.00	524.29K	71.95	72.43	4.65	262.14K	72.69	73.77	5.79
R18(m=16)-3x3x3x	81.92K	52.77	53.07	0.00	49.15K	64.93	65.67	9.59	36.86K	66.23	67.96	11.57
R18(m=16)-4x4x4x	81.92K	52.19	52.20	0.00	65.54K	65.62	66.22	10.46	65.54K	67.82	69.16	12.66
R18(m=16)-5x5x5x	81.92K	50.38	50.65	0.00	81.92K	66.10	66.63	11.74	102.40K	70.17	70.64	14.46
R18(m=16)-6x6x6x	81.92K	50.60	51.53	0.00	98.30K	66.74	67.11	11.30	147.46K	70.67	72.09	14.49
R18(m=16)-7x7x7x	81.92K	50.93	49.07	0.00	114.69K	66.59	67.89	13.50	200.70K	72.08	73.33	16.74

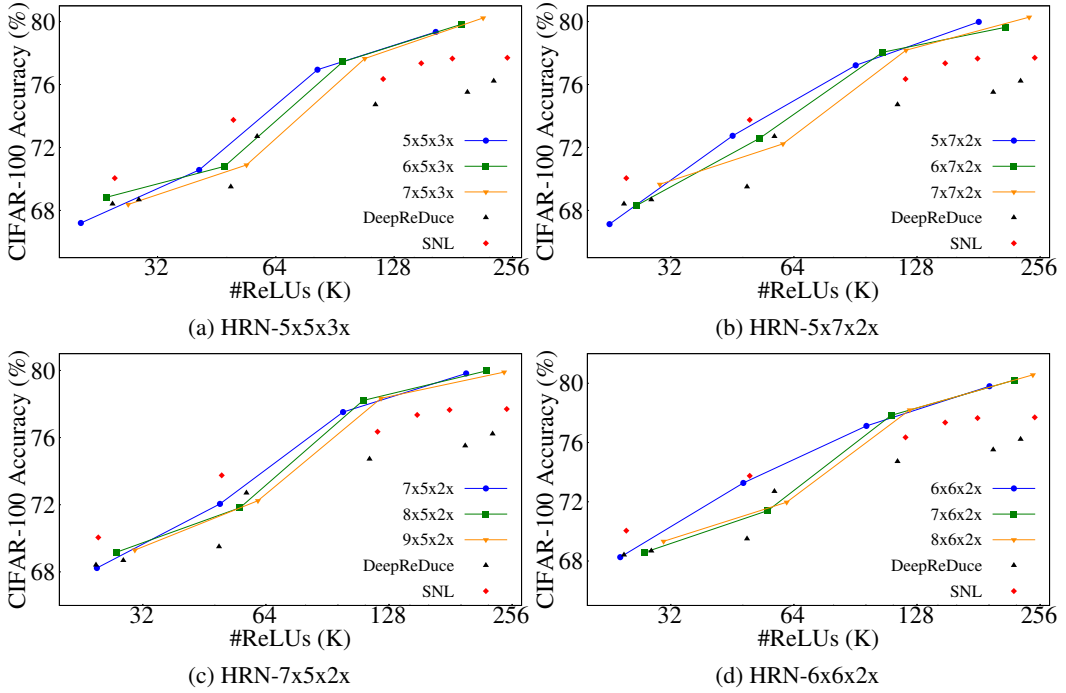


Figure 14: Effect of increasing  $\alpha$  in HRN networks: The ReLU-efficiency of networks with higher  $\alpha$  does not improve, in fact it significantly reduces at lower ReLU counts.

It remains intriguing to examine if the ReLUs’ criticality order in baseline networks, such as ResNet18, remains consistent when the network width is modified, specifically in the *BaseCh*, *StageCh*, and HRN variations. To this end, we compute the stagewise criticality metric for ResNet18 *BaseCh* and *StageCh* networks (Table 8), and HRN networks with  $\alpha$  values between 2 and 7 (Table 9). Interestingly, the criticality order of the standard ResNet18 is *preserved* in *BaseCh* and *StageCh* models, and all HRNs, except for those with  $\alpha=2$  (HRN-2x5x3x, HRN-2x5x2x, HRN-2x6x2x, and HRN-2x7x2x). Specifically, the criticality order of Stage2 and Stage3 is shuffled in HRNs with  $\alpha=2$ , while the most and least critical stages remain unchanged (i.e.,  $S_3 > S_2 > S_4 > S_1$ ). To account for this altered criticality order, we recompute  $\alpha$ ,  $\beta$ , and  $\gamma$  using Algorithm 1, and obtain two HRNs, HRN-2x6x3x and HRN-2x9x2x; however, the criticality order in these two HRNs does not adapt to the altered criticality order (highlighted as green in Table 9).

## C Additional Experimental Results

### C.1 ReLU Equalization through Network’s Depth in BaseCh Networks

ReLU equalization through width in HybReNets results in two simultaneous effects. Firstly, it increases the network’s complexity per unit of nonlinearity, measured as parameters and FLOPs per units of ReLU. Secondly, it aligns the distribution of ReLUs in their criticality order. However, to analyze the significance of these effects independently, we apply ReLU equalization through depth and augment the base channel counts to increase the parameters and FLOPs per units of ReLU.

In this study, we use the classical ResNet18 with  $m=16$  and fixed  $\alpha=\beta=\gamma=2$ ; however, set the stage compute ratios ( $\phi_1, \phi_2, \phi_3$ , and  $\phi_4$ ) as design hyperparameters. Now, we employ Algorithm 1 for ReLU equalization and solve compound inequalities to obtain the depth hyperparameters. Specifically, we determine the depth hyperparameters  $(\phi_1, \phi_2, \phi_3, \phi_4) \in \{(1,5,5,3); (1,5,7,2); (1,6,6,2); \text{ and } (1,7,5,2)\}$  that correspond to the minimum values enabling ReLU equalization. It is worth noting that the sum of all the stage compute ratio results in a network’s global depth of 14. Next, we increase the parameters and FLOPs per unit of ReLU by varying  $m \in \{16, 32, 64, 128, \text{ and } 256\}$ . The experimental results are shown in Figure 15, where we compare the ReLU and FLOPs efficiency with

Table 9: Evaluating Stagewise ReLU criticality in (ResNet18-based) HRN networks with  $\alpha$  values spanning 2 to 7, on the CIFAR-100 dataset. Criticality metrics ( $C_k$ ) for each stage are determined using the method in [17]. Notably, the criticality order of all HRN networks, except the smallest one with  $\alpha=2$ , aligns with the original ResNet18 order ( $S_3 > S_2 > S_4 > S_1$ ). HRNs with the minimum  $\alpha$ ,  $\beta$ , and  $\gamma$  required for (full) ReLU equalization are emphasized in gray.

Networks	Stage1				Stage2				Stage3				Stage4			
	#ReLUs	Acc(%)	+KD(%)	$C_k$	#ReLUs	Acc(%)	+KD(%)	$C_k$	#ReLUs	Acc(%)	+KD(%)	$C_k$	#ReLUs	Acc(%)	+KD(%)	$C_k$
HRN-2x7x2x	81.92K	52.14	53.39	<b>0.00</b>	32.77K	61.63	61.59	<b>6.42</b>	57.34K	68.44	69.82	<b>12.37</b>	28.67K	62.15	63.40	<b>7.91</b>
HRN-3x7x2x	81.92K	51.61	53.29	<b>0.00</b>	49.15K	64.46	65.26	<b>9.11</b>	86.02K	69.88	70.77	<b>12.80</b>	43.01K	63.10	64.17	<b>8.36</b>
HRN-4x7x2x	81.92K	51.28	49.42	<b>0.00</b>	65.54K	65.93	66.47	<b>12.72</b>	114.69K	70.94	72.16	<b>16.32</b>	57.34K	63.70	64.77	<b>11.56</b>
HRN-5x7x2x	81.92K	49.82	48.36	<b>0.00</b>	81.92K	66.17	67.59	<b>14.13</b>	143.36K	71.40	72.18	<b>16.83</b>	71.68K	64.10	65.35	<b>12.60</b>
HRN-6x7x2x	81.92K	51.23	48.48	<b>0.00</b>	98.30K	66.88	68.06	<b>14.20</b>	172.03K	71.86	72.73	<b>16.91</b>	86.02K	64.15	65.75	<b>12.64</b>
HRN-7x7x2x	81.92K	50.11	52.40	<b>0.00</b>	114.69K	66.92	68.29	<b>11.40</b>	200.70K	71.69	73.16	<b>14.32</b>	100.35K	63.82	65.53	<b>9.51</b>
HRN-2x6x2x	81.92K	52.29	53.19	<b>0.00</b>	32.77K	61.62	62.00	<b>6.90</b>	49.15K	67.36	69.51	<b>12.43</b>	24.58K	61.64	63.25	<b>8.04</b>
HRN-3x6x2x	81.92K	52.50	52.80	<b>0.00</b>	49.15K	64.50	65.64	<b>9.78</b>	73.73K	68.61	70.96	<b>13.44</b>	36.86K	62.77	64.09	<b>8.77</b>
HRN-4x6x2x	81.92K	53.23	53.32	<b>0.00</b>	65.54K	65.74	66.03	<b>9.48</b>	98.30K	70.47	71.54	<b>13.22</b>	49.15K	63.59	64.82	<b>8.76</b>
HRN-5x6x2x	81.92K	50.79	51.64	<b>0.00</b>	81.92K	66.89	67.27	<b>11.48</b>	122.88K	70.33	71.50	<b>14.18</b>	61.44K	63.97	64.94	<b>9.97</b>
HRN-6x6x2x	81.92K	50.01	50.59	<b>0.00</b>	98.30K	66.57	67.94	<b>12.58</b>	147.46K	71.18	72.59	<b>15.51</b>	73.73K	64.13	65.39	<b>10.95</b>
HRN-7x6x2x	81.92K	51.01	49.64	<b>0.00</b>	114.69K	66.74	68.57	<b>13.58</b>	172.03K	71.84	72.84	<b>16.18</b>	86.02K	64.54	65.16	<b>11.36</b>
HRN-2x5x2x	81.92K	52.03	53.05	<b>0.00</b>	32.77K	61.60	61.76	<b>6.82</b>	40.96K	66.64	68.29	<b>11.75</b>	20.48K	61.02	62.58	<b>7.71</b>
HRN-3x5x2x	81.92K	53.43	52.61	<b>0.00</b>	49.15K	64.57	65.71	<b>9.97</b>	61.44K	68.40	69.93	<b>12.98</b>	30.72K	62.32	63.42	<b>8.51</b>
HRN-4x5x2x	81.92K	52.65	52.33	<b>0.00</b>	65.54K	65.60	66.89	<b>10.86</b>	81.92K	69.81	70.85	<b>13.61</b>	40.96K	63.14	63.94	<b>8.95</b>
HRN-5x5x2x	81.92K	49.15	51.16	<b>0.00</b>	81.92K	66.26	67.47	<b>11.18</b>	102.40K	70.15	71.69	<b>14.85</b>	51.20K	63.55	64.67	<b>10.26</b>
HRN-6x5x2x	81.92K	49.00	52.10	<b>0.00</b>	98.30K	66.56	68.00	<b>11.59</b>	122.88K	71.33	71.85	<b>14.10</b>	61.44K	63.59	64.89	<b>9.59</b>
HRN-7x5x2x	81.92K	51.58	51.93	<b>0.00</b>	114.69K	66.94	67.89	<b>11.45</b>	143.36K	70.79	72.87	<b>14.79</b>	71.68K	64.02	65.23	<b>9.86</b>
HRN-2x5x3x	81.92K	52.36	53.68	<b>0.00</b>	32.77K	61.39	61.30	<b>5.97</b>	40.96K	66.78	68.17	<b>11.17</b>	30.72K	62.01	63.83	<b>7.99</b>
HRN-3x5x3x	81.92K	51.05	52.89	<b>0.00</b>	49.15K	64.64	65.10	<b>9.30</b>	61.44K	68.87	70.14	<b>12.93</b>	46.08K	63.66	64.32	<b>8.74</b>
HRN-4x5x3x	81.92K	51.57	50.62	<b>0.00</b>	65.54K	65.66	66.06	<b>11.52</b>	81.92K	69.12	70.13	<b>14.33</b>	61.44K	63.64	65.58	<b>11.21</b>
HRN-5x5x3x	81.92K	50.22	52.41	<b>0.00</b>	81.92K	66.42	67.55	<b>11.12</b>	102.40K	70.15	70.97	<b>13.42</b>	76.80K	64.21	65.59	<b>9.73</b>
HRN-6x5x3x	81.92K	50.28	50.45	<b>0.00</b>	98.30K	65.95	67.61	<b>12.45</b>	122.88K	70.68	71.29	<b>14.88</b>	92.16K	64.37	65.87	<b>11.23</b>
HRN-7x5x3x	81.92K	50.12	50.31	<b>0.00</b>	114.69K	66.85	67.95	<b>12.66</b>	143.36K	71.20	71.87	<b>15.23</b>	107.52K	64.72	65.58	<b>11.01</b>
HRN-2x9x2x	81.92K	51.86	53.22	<b>0.00</b>	32.77K	61.13	61.65	<b>6.60</b>	73.73K	69.46	70.28	<b>12.63</b>	36.86K	62.53	64.25	<b>8.57</b>
HRN-2x6x3x	81.92K	52.75	52.85	<b>0.00</b>	32.77K	61.33	61.44	<b>6.73</b>	49.15K	67.36	68.76	<b>12.11</b>	36.86K	62.69	64.59	<b>9.12</b>

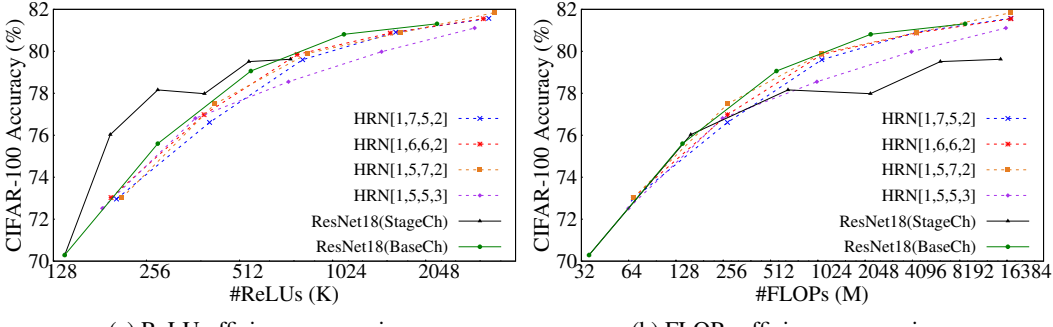


Figure 15: ReLU and FLOPs efficiency when network’s ReLU is equalized, in their criticality order, through depth, by altering the stage compute ratios (their modified values are shown in bracket  $[]$ ). The network’s complexity per units of nonlinearity (ReLUs) is increased by augmenting  $m \in \{16, 32, 64, 128, 256\}$ . ReLU and FLOPs efficiency of these HRNs are either similar or worse compared to *BaseCh* networks, *suggesting the effectiveness of ReLU equalization through width* (by altering  $\alpha$ ,  $\beta$ , and  $\gamma$ )

*BaseCh* and *StageCh* networks. Interestingly, we observe that the ReLU and FLOPs efficiency of the networks derived above are either similar or worse compared to *BaseCh* networks. For instance, HRN[1,5,5,3] exhibits inferior ReLU/FLOPs efficiency at higher ReLU/FLOPs count compared with *BaseCh* networks. Consequently, this underscores the significance of ReLU equalization through width adjustment, by altering  $\alpha$ ,  $\beta$ , and  $\gamma$ , and *demonstrates that ReLU equalization alone does not yield the desired benefits in HybReNets*.

## C.2 Additional Results for Capacity-Criticality-Tradeoff

We conducted additional experiments on different HybReNets to further investigate the ‘‘Capacity-Criticality Tradeoff’’ phenomenon shown in Figure 5. In particular, for each set of experiments, we chose three HRN networks with reduced values of  $\alpha$ , with a fixed  $(\beta, \gamma)$ , and employ DeepReDuce and SNL ReLU optimization techniques. The results are presented in Figure 16. Notably, lowering  $\alpha$  results in higher fraction of network’s ReLUs in Stage1, as shown in Table 9. For instance, HRN-6x6x2x, HRN-4x6x2x, and HRN-2x6x2x have the Stage1 fraction of network’s total ReLU count

as 20.4%, 27.8%, and 43.5%, respectively. Our observations on both DeepReDuce and SNL are consistent with those in Figure 5. Precisely, HRN-6x6x2x and HRN-4x6x2x outperform HRN-2x6x2x at higher ReLU counts; whereas, HRN-2x6x2x is superior at lower ReLU counts (Figure 16(b,e)).

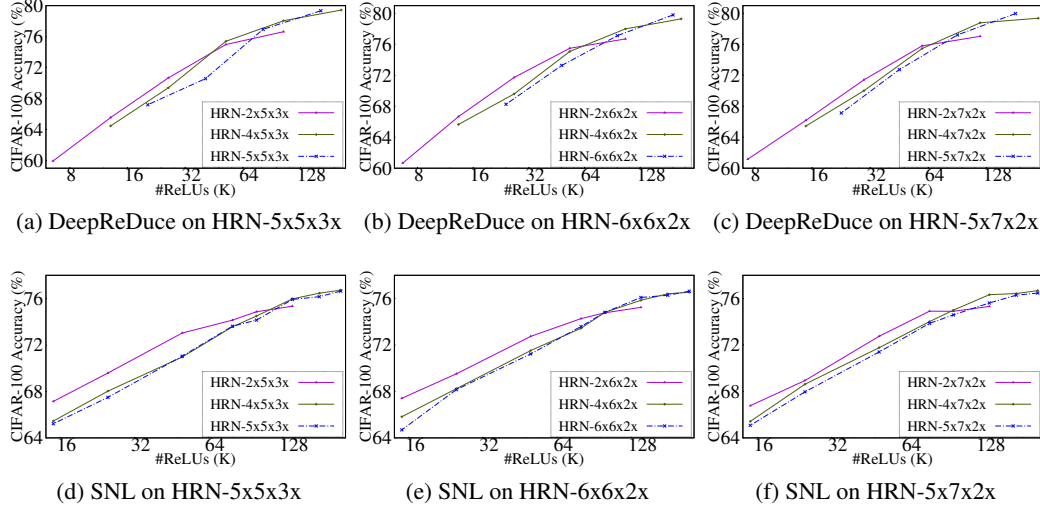


Figure 16: Capacity-Criticality Tradeoff in HRN networks for coarse/fine-grained ReLU optimization DeepReDuce/SNL. HRN networks with decreasing value of  $\alpha$  has higher proportion of Stage1 (non-critical) ReLUs, and exhibit superior performance at lower ReLU counts.

### C.3 Explanation and Intuition for Capacity-Criticality Tradeoff

We have observed that networks with a higher percentage of non-critical (Stage1) ReLUs tend to have lower overall ReLU counts. This pattern is consistent across both traditional networks like ResNet18 and WRN22x8, as well as HRN networks. For example, WRN22x8 and ResNet18, used in SNL [20] and SENet [21] for advancing the ReLU-accuracy Pareto frontier at different ReLU counts, contain 1392.6K and 557K ReLUs, respectively. Also, in HybReNet, when we decrease the value of  $\alpha$  while keeping  $\beta$  and  $\gamma$ , the total ReLU count in the network decreases, and the percentage of Stage1 ReLUs increases. For instance, HRN-6x6x2x, HRN-4x6x2x, and HRN-2x6x2x have ReLU counts of 401.4K, 294.9K, and 188.4K, respectively. *This raises the fundamental question of what drives the better performance at lower ReLU counts* — the proportion of ReLUs in Stage1 or the total number of ReLUs in the network? Further investigation is required to shed light on this issue.

To pinpoint the primary factor influencing PI performance at lower ReLU counts, we conducted an experiment with ResNet34 and a ResNet18 variant (ResNet18( $m = 16$ )-4x4x4x), having a uniform ReLU distribution, as employed in [14] and Sphynx [19]. Results are shown in Table 10. Evidently, despite having  $3.5 \times$  fewer ReLUs, the performance of ResNet18( $m=16$ )-4x4x4x is inferior to that of ResNet34 when ReLU counts are below 50K. This is due to a lower percentage (29.41%) of Stage1 ReLUs in comparison to ResNet34 (47.46%). Likewise, the improved performance of ResNet18 over WRN22x8 at lower ReLU counts, as seen in previous studies [21, 20], cannot be ascribed to the total ReLU count. Instead, it is attributed to the proportion of Stage1 ReLUs, with ResNet18 having 58.8% and WRN22x8 having 48.2%.

To gain a better understanding of why having a higher fraction of Stage1 ReLUs is preferable for achieving superior performance at lower ReLU counts, we examined the ReLU dropping strategies employed in the prevalent ReLU optimization techniques. Specifically, we examined the strategies employed by DeepReDuce [17], SNL [20], and SENet [21], and found that they consistently demonstrate that Stage1 ReLUs are the least critical, and as such, all Stage1 ReLUs are dropped first to achieve very low ReLU counts. Consequently, networks with a greater proportion of non-critical ReLUs will drop a lower fraction of their critical ReLUs when aiming for very low ReLU counts, as opposed to networks with a lower proportion of non-critical ReLUs. This can be observed in Figure 17. In particular, regardless of the total ReLU count of the network, WRN22x8 (ResNet18( $m=16$ )-4x4x4x) drops a higher fraction of their critical ReLUs compared to ResNet18 (ResNet34) in order to

Network	#ReLUs	Stage1(%)	180K	100K	50K	15K
ResNet34	966.7K	47.46	76.35%	74.55%	72.07%	66.46%
4x4x4x	278.5K	29.41	77.08%	75.03%	71.38%	64.77%

Table 10: Performance comparison (using SNL ReLU optimization) of ResNet34 and ResNet18 variant (ResNet18( $m=16$ )-4x4x4x), having a uniform distribution of ReLUs. Stage1(%) is the fraction of network’s ReLU in Stage1. *Despite having 3.5× fewer ReLUs, the performance of 4x4x4x remains inferior to ResNet34 when the ReLU count falls below 50K.* Thus, the key determinant for the superior performance at very low ReLU count is the fraction of non-critical ReLUs, rather than the network’s total ReLU count.

attain a ReLU count of 25K. Thus, *dropping a higher fraction of critical ReLUs lead to a significant loss in accuracy and results in inferior performance.*

Further, we note that the aforementioned observation resonates with the findings made in [46] — neurons in the middle layers of a network (i.e., Stage2 and Stage3) *exhibit fragile co-adaption*, which is difficult to re-learn. Consequently, dropping more ReLUs from these stages in a network with lower fraction of non-critical (Stage1) ReLUs would disrupt the fragile co-adaption and significantly reduce performance.

#### C.4 SNL ReLU Optimization on HybReNet Networks

We employ SNL ReLU optimization [20] on the four distinct HRN configurations – HRN-5x5x3x, HRN-5x7x2x, HRN-6x6x2x, and HRN-7x5x2x – in order to assess the efficacy of fine-grained ReLU optimization in the context of HRNs. Results are presented in Figure 18. Evidently, the HRNs with SNL ReLU optimization are inferior to the vanilla SNL, employed on WRN22x8 (for #ReLUs  $> 100K$ ) and ResNet18 (for #ReLUs  $\leq 100K$ ). However, employing SNL on ReLU-Thinned HRNs results in an accuracy boost, up to 3%, across all the ReLU counts. This leads to at par performance with vanilla SNL, thereby emphasizing the significance of ReLU Thinning even for the fine-grained ReLU optimization.

Notice that aforementioned findings are consistent with the observations made in Figure 6 and Table 4, demonstrating the limitations of SNL when the distribution of ReLU altered. Specifically, when the proportion of network’s ReLU belonging to Stage1 decreases and those in the other stages increase. *This imply that the benefits of fine-grained ReLU optimization may contingent on a higher proportion of non-critical (Stage1) ReLUs.* Further, to assess the efficacy of ReLU Thinning in the context of fine-grained ReLU optimization, we compare the total number of ReLUs within a network before and after the implementation of the technique. For instance, in the case of a 50K ReLU budget allocated to the HRN-5x7x2x model, the SNL algorithm identifies 50K essential ReLUs from an initial pool of 363.5K ReLUs, subsequently eliminating 312.5K ReLUs. Conversely, when employing the Thinned HRN network, the SNL algorithm detects the 50K critical ReLUs from a diminished pool of 181.25K ReLUs and drops 131.25K ReLUs, given that Thinning eliminates half of the network’s ReLUs from alternating layers, irrespective of their criticality. *This results into an accuracy boost of 2.44% (on CIFAR-100).* Thus, ReLU Thinning demonstrates its effectiveness as a method for reducing the search space required to identify critical ReLUs.

## D Detailed Analysis of ReLU-Accuracy Pareto Points

In this section we detailed the ReLU optimization steps used in ReLU-Accuracy Pareto frontier, transitioning from higher to lower accuracy points, as shown in Figure 10 (a,b) and the Table 6. When employing ReLU-reuse, we fixed  $m=16$ ; however, the network’s FLOPs count reduces due to the group-wise convolution. For instance, the HRN-2x6x3x model with a ReLU-reuse factor of four has 370.1M FLOPs, compared to the original HRN-2x6x3x model ( $m=16$ ) with 527.4M FLOPs, when

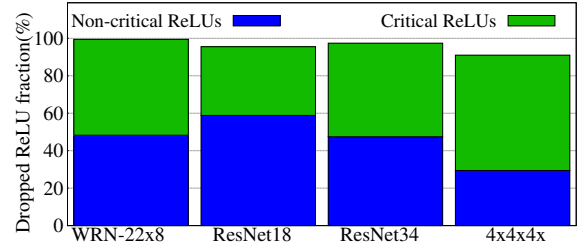


Figure 17: Networks with higher fraction of non-critical (Stage1) ReLUs, ResNet18 (ResNet34) drops lesser fraction of their (remaining stages) critical ReLUs, compared to WRN22x8 (4x4x4x), to achieve a ReLU count of 25K, *regardless of the their absolute ReLU counts.*

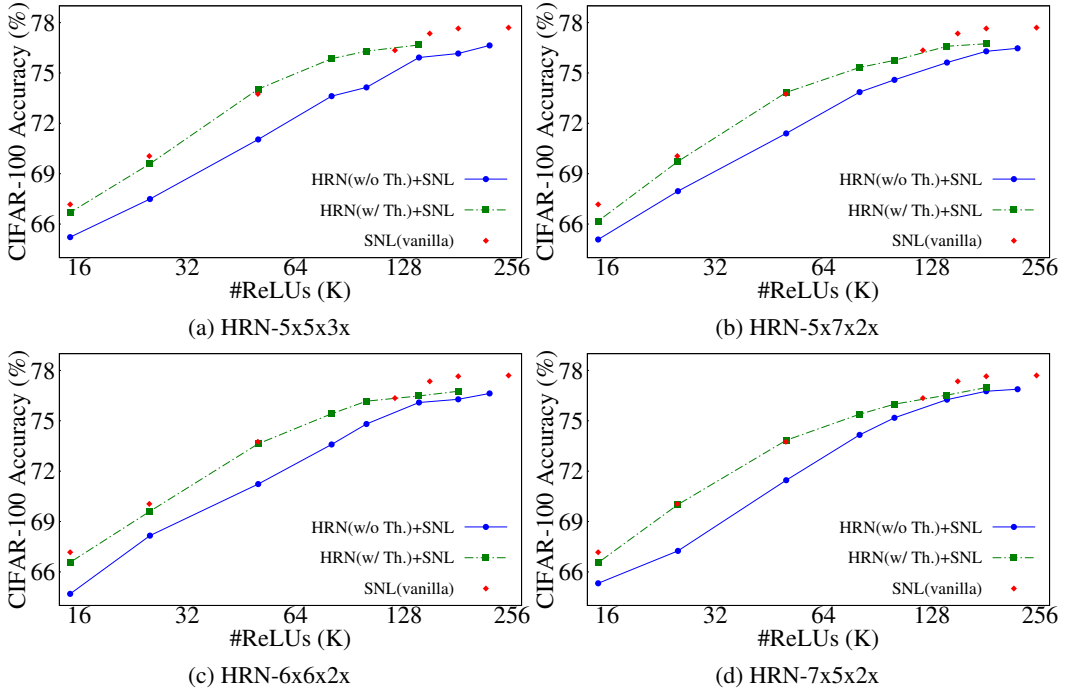


Figure 18: HybReNets with fine-grained ReLU optimization: HRNs with SNL (fine-grained) ReLU optimization exhibit a suboptimal ReLU-Accuracy tradeoff compared to the vanilla SNL approach used in traditional networks such as ResNet18 and WRN22x8. However, employing ReLU-Thinning (a coarse-grained ReLU optimization step used in DeepReDuce), prior to SNL optimization yields performance on par with the vanilla SNL method, *thus highlighting the significance of ReLU Thinning in ReLU optimization, even in the context of fine-grained ReLU optimization.*

used on CIFAR-100 (see Table 12). Nonetheless, because of specific implementation constraints of group convolution in Microsoft SEAL [47], we calculated the HE latency without taking into account the FLOPs reduction resulting from the use of group convolution in ReLU-reuse.

Table 11: Network configurations and ReLU optimization steps employed for the HybReNet (TinyImageNet) points in Table 6. Re2 denotes ReLU-reuse, a key method in achieving significantly reduced ReLU-counts.

HybReNet	$m$	ReLU optimization steps			#ReLU	#FLOPs	Accuracy(%)		Acc./ReLU
		Culled	Thinned	Re2			KD[34]	DKD[35]	
5x5x3x	16	NA	S1+S2+S3+S4	NA	653.3K	4216.4M	65.76	67.58	0.10
2x5x3x	32	S1	S2+S3+S4	NA	417.8K	2841.7M	64.11	66.10	0.16
5x5x3x	8	NA	S1+S2+S3+S4	NA	326.6K	1055.4M	61.92	64.92	0.20
2x5x3x	8	S1	S2+S3+S4	NA	104.4K	178.9M	56.37	58.90	0.56
2x5x3x	16	S1	S2+S3+S4	4	52.2K	486.3M	53.13	54.46	1.04

## E Discussion

### E.1 FLOPs-efficiency Restricts the Flexibility for Widening Classical Neural Networks

Classical networks follow a convention of doubling the filter count when downsampling feature maps by a factor of two to avoid representational bottlenecks [48]. This results in a fixed stagewise channel multiplication factors (shown in Figure 2) of  $\alpha = \beta = \gamma = 2$  for most classical networks. Even for designing state-of-the-art FLOPs-efficient vision models, RegNet [31], stagewise channel multiplication factor are restricted as  $1.5 \leq (\alpha, \beta, \gamma) \leq 3$ . Conventional network design paradigms prioritize

Table 12: Network configurations and ReLU optimization steps employed for the Pareto points in Figure 10 (a,b), along with and the HybReNet points used for the comparison with SOTA PI methods and ConvNeXt-V2 [42] as illustrated in Table 12. Re2 denotes ReLU-reuse, a key method in achieving significantly reduced ReLU-counts.

	Nets	m	ReLU optimization steps			#ReLU	#FLOPs	Accuracy(%)		Acc./ReLU	
			Culled	Thinned	Re2			KD[34]	DKD[35]		
CIFAR-100	HybReNet	4x6x3x	16	NA	S1+S2+S3+S4	NA	317.4K	2061.1M	80.14	81.36	0.26
		2x6x3x	16	S1	S2+S3+S4	NA	134.1K	527.4M	78.80	79.56	0.59
		2x6x3x	8	S1	S2+S3+S4	NA	67.1K	132.2M	74.84	76.91	1.15
		2x6x3x	16	S1	S2+S3+S4	4	33.5K	370.1M	70.93	73.89	2.21
		2x6x3x	16	S1	S2+S3+S4	8	16.6K	394.8M	68.17	69.70	4.19
		2x6x3x	16	S1	S2+S3+S4	16	8.3K	413.4M	62.44	64.65	7.78
		4x6x3x	16	NA	S1+S2+S3+S4	NA	1269.8K	8244.2M	68.90	70.29	0.06
TinyImageNet	HybReNet	4x6x3x	12	NA	S1+S2+S3+S4	NA	952K	4638.8M	68.16	69.15	0.07
		2x6x3x	16	S1	S2+S3+S4	NA	536.6K	2109.4M	66.29	67.48	0.13
		2x6x3x	12	S1	S2+S3+S4	NA	402K	1187.5M	64.51	65.77	0.16
		2x6x3x	8	S1	S2+S3+S4	NA	268.3K	528.6M	60.97	64.02	0.24
		2x6x3x	16	S1	S2+S3+S4	4	134.1K	1480.1M	57.84	61.52	0.46
		2x6x3x	16	S1	S2+S3+S4	8	67.1K	1579.2M	54.47	56.24	0.84
		2x6x3x	16	S1	S2+S3+S4	16	33.5K	1653.5M	49.13	49.96	1.49
ConvNeXt	ConvNeXt	T	96	S1	S2+S3+S4	NA	1622K	11801M	68.32	69.85	0.04
		N	80	S1	S2+S3+S4	NA	1278K	9080.2M	66.73	68.75	0.05
		P	64	S1	S2+S3+S4	NA	720.9K	3435.7M	65.42	67.08	0.09
		F	48	S1	S2+S3+S4	NA	540.7K	1935M	64.23	65.72	0.12
		A	40	S1	S2+S3+S4	NA	450.6K	1345.1M	63.23	64.08	0.14

FLOPs efficiency, which is why the stagewise multiplication factor is typically conservative. The quadratic dependency of FLOPs on the channel counts (see Figure 2), along with the multiplicative effect of stagewise multiplication factors, means that even a small increase in these factors can lead to a significant increase in FLOPs count, thus hampering FLOPs efficiency.

In contrast, we observed that networks having a higher value of  $\beta$ , along with lower values of  $\alpha$  and  $\gamma$ , provide a better FLOPs-ReLU-Accuracy tradeoff compared to the classical networks with  $\alpha = \beta = \gamma = 2$ . Notably, HRN-2x5x2x, HRN-2x5x2x, HRN-2x6x2x, and HRN-2x7x2x outperform ResNet18 baseline networks, with both  $m=64$  and  $m=32$ , and exhibit a better FLOPs-ReLU-Accuracy balance.

## E.2 HybReNets Achieves FLOP-ReLU-Accuracy Balance by Limiting FLOPs Expansion in Deeper Layers

In Appendix A, the derivation steps for ReLU equalization on a four-stage network shows that  $\beta$  and  $\gamma$  values are bounded by  $\beta\gamma < 16$  and  $\gamma < 4$ . These constraints effectively limit the growth of FLOPs in deeper layers, making HRN networks more efficient in terms of computation than their StageCh counterparts, which exhibit homogeneous sets of  $\alpha$ ,  $\beta$ , and  $\gamma$ , leading to an undesirably rapid growth of FLOPs in deeper layers. To visualize this, we compute the normalized FLOPs in ResNet18 based StageCh networks, in contrast with HRNs. We observed that the normalized FLOPs in Stage3 and Stage4 of ResNet18 are expressed as  $\frac{\alpha^2\beta^2}{16}$  and  $\frac{\alpha^2\beta^2\gamma^2}{64}$  (respectively); thus, network with  $\gamma=2$  would have equal FLOPs in Stage3 and Stage4. This is evident from the (normalized) stagewise FLOPs ratio for HRN-5x7x2x, HRN-7x5x2x, and HRN-6x6x2x networks in Table 13.

In conclusion, constraints on  $\gamma$ , which must be less than 4, keeps the ReLU count of Stage4 lower than that of Stage3 (most critical stage), which in turn restrict the FLOPs count of Stage4. While further restricting  $\alpha$  and  $\beta$  values can reduce the network's FLOPs, this would also reduces the proportion of the most significant (Stage3) ReLUs. As a result, a criticality-aware network design streamline both the ReLU and FLOPs in networks and prevent superfluous FLOPs (in contrast with StageCh networks), and maximize the utilization of the network's FLOPs for a given ReLU count.

Table 13: Depiction of stagewise FLOPs and ReLU trend variation, with  $\alpha, \beta$ , and  $\gamma$ , in StageCh and HRN networks. The least and most critical ReLUs are colored in **red** and **blue**, respectively. Evidently, in contrast with StageCh network, **ReLU-equalization in HRNs restrict the growth of FLOPs in deeper layers** and networks achieve ReLU efficiency at par with StageCh network; however, with fewer FLOPs. This way HRN networks achieve FLOPs-ReLU-accuracy balance.

	Stage1	Stage2	Stage3	Stage4	$(\alpha, \beta, \gamma)=2$	$2 < (\alpha, \beta, \gamma) < 4$	$(\alpha, \beta, \gamma)=4$	$(\alpha, \beta, \gamma) > 4$
FLOPs	1	$\frac{\alpha^2}{4}$	$\frac{\alpha^2\beta^2}{16}$	$\frac{\alpha^2\beta^2\gamma^2}{64}$	Layerwise FLOPs	constant	increasing ( $\uparrow$ )	increasing ( $\uparrow\uparrow$ )
ReLUs	1	$\frac{\alpha}{4}$	$\frac{\alpha\beta}{16}$	$\frac{\alpha\beta\gamma}{64}$	Layerwise ReLUs	decreasing ( $\downarrow\downarrow$ )	decreasing ( $\downarrow$ )	constant
	$(\alpha, \beta, \gamma) = (2, 2, 2)$				$(\alpha, \beta, \gamma) = (3, 3, 3)$			
FLOPs	64	64	64	64	Stage1 64	Stage2 144	Stage3 324	Stage4 729
ReLUs	<b>64</b>	32	<b>16</b>	8	<b>64</b>	48 <b>36</b>	27 <b>64</b>	<b>64</b>
	$(\alpha, \beta, \gamma) = (4, 4, 4)$				$(\alpha, \beta, \gamma) = (6, 6, 6)$			
	HRN-5x7x2x				HRN-7x5x2x			
FLOPs	64	400	4900	4900	Stage1 64	Stage2 784	Stage3 4900	Stage4 4900
ReLUs	<b>64</b>	80	<b>140</b>	70	<b>64</b>	112 <b>140</b>	70 <b>64</b>	<b>64</b>
	HRN-6x6x2x				HRN-5x5x3x			
	HRN-5x5x3x				HRN-5x5x3x			
FLOPs	64	400	2500	5625	Stage1 64	Stage2 80	Stage3 <b>100</b>	Stage4 75
ReLUs	<b>64</b>	<b>80</b>	<b>144</b>	<b>75</b>				

### E.3 Understanding Accuracy Plateau in StageCh Networks through Deep Double Descent Phenomenon

A distinct trend in the ReLU-Accuracy tradeoff has been observed (see Figure 3(a,b)) as the width of models is increased by augmenting  $\alpha, \beta$ , and  $\gamma$ . Specifically, accuracy initially increases with increasing values of  $\alpha, \beta$ , and  $\gamma$ , reaches a saturation point, and then increases again at higher ReLU counts. This trend is more prominent in models with smaller depth, such as ResNet18, and disappears in deeper models like ResNet56, where performance does not improve after saturation. The observed saturation trend in ReLU-accuracy trade-off can be explained by the “model-wise deep double descent” phenomenon, which becomes more pronounced with higher label noise [49–51]. In the presence of label noise, a U-shaped curve appears in the classical (under-parameterized) regime due to a bias-variance tradeoff, and in the over-parameterized regime, accuracy improves due to the regularization enabled by the strong inductive bias of the network. However, with zero label noise, the test error plateaus around the interpolation threshold, resulting in a flat trend similar to the one shown in Figure 3(a,b), instead of a U-shaped curve.

### E.4 Why RegNet and ConvNeXt Models are Selected for Our Case Study?

RegNets are models that have been designed using a semi-automated network design method, which are parameterized by the stage compute ratio  $(\phi_1, \phi_2, \phi_3, \phi_4)$ , base channel count ( $m$ ), and stagewise channel multiplication factors as  $1.5 \leq (\alpha, \beta, \gamma) \leq 3$ . On the other hand, ConvNeXts are redesigned ResNets with modified values of  $m$  and  $\phi_1, \phi_2, \phi_3, \phi_4$ . For example, the ConvNeXt-T model has a stage compute ratio of  $[3, 3, 9, 3]$ , which is different from the  $[3, 4, 6, 3]$  ratio used in ResNet34, and a base channel count of  $m=96$ , which is higher than the  $m=64$  used in ResNet34. As a result, the unconstrained design choices in RegNets and the modified depth and width in ConvNeXt models make them suitable for our case study, where we investigate their impact on ReLU distribution and the FLOPs-ReLU-Accuracy balance.

### E.5 Potential of ReLU Equalization as a Unified Network Design Principle

The field of deep learning has witnessed remarkable progress in recent years, largely due to the development of increasingly sophisticated neural network architectures. Traditionally, researchers have relied on manual network design techniques such as ResNet [26], ResNeXt [52], ConvNeXt [45], etc., or neural architecture search methods [53–56]. However, *these approaches have their limitations*. Manual techniques often lead to suboptimal models as design choices increase, while neural architecture search lacks interpretability and may not generalize beyond restricted settings. Additionally, both methods require significant computational resources to find optimal design hyperparameters when networks are designed from scratch.

A semi-automated design technique like RegNets [31] offers interpretable network design and automates the process of finding the optimal population of networks that can generalize across a wide range of settings. However, it requires training thousands of models in each iteration to narrow down the search space and assess the quality of the design space, making it expensive when models are

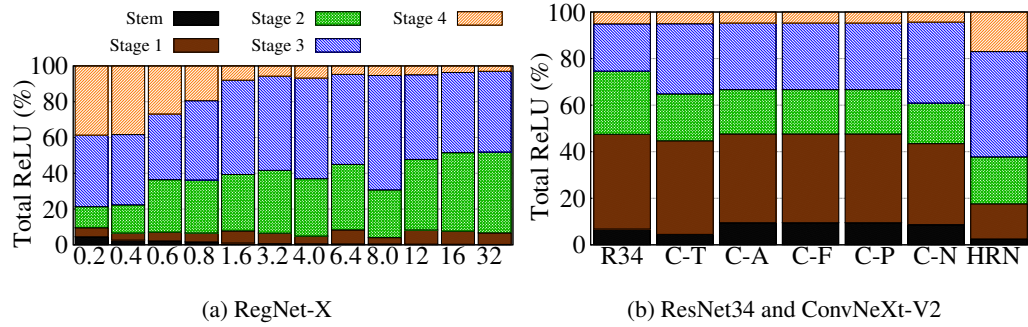


Figure 19: Analyzing the distribution of ReLU in RegNet-X [31] and ConvNeXt-V2 [42] architectures reveals *interesting patterns*. In all RegNet-X models, ReLUs are arranged precisely according to their criticality order. In contrast, the ConvNeXt models, including their T, A, F, P, and N variations, have a higher proportion of network’s ReLU in the most-critical stage (Stage3), while that of the less crucial ReLUs (Stage1) is reduced due to the modification of depth and width design parameters. In contrast, the distribution of ReLUs in the HRN-4x6x3x model strictly adheres to their criticality order.

designed from scratch. Here, we emphasize that RegNet networks’ width and depth are explained by a sophisticated quantized linear function that equalizes the networks’ ReLU in their order of criticality (see Figure 19(a)).

Likewise, ReLUs’ distribution in all but Stage1, of ConvNeXt models follow their criticality order. Precisely, ConvNeXt-T (ConvNext-N) model increases the proportion of most-critical (Stage3) ReLUs from 20.3% to 30.2%(34.8%) in ResNet34; while, reducing the proportion of less critical ReLUs (see Figure 19(b)). Furthermore, as evident from the comparative summary of stagewise channel allocation in ConvNeXt models and HRNs (with  $\alpha=2$ ), the channel counts in the deeper stages of both models (ConvNeXt and HRNs) are an exact match, where HRNs tend to allocate fewer channels during the initial stages. This demonstrate the generality of ReLU equalization as a design principle even for designing FLOPs-efficient models.

- ConvNext V2-T  $m=96$  [96, 192, 384, 768]
- ConvNext V2-N  $m=80$  [80, 160, 320, 640]
- ConvNext V2-P  $m=64$  [64, 128, 256, 512]
- ConvNext V2-F  $m=48$  [48, 96, 192, 384]
- ConvNext V2-A  $m=40$  [40, 80, 160, 320]
- HRN-2x6x2x  $m=32$  [32, 64, 384, 768]
- HRN-2x5x2x  $m=32$  [32, 64, 320, 640]
- HRN-2x5x3x  $m=16$  [16, 32, 160, 480]
- HRN-2x6x2x  $m=16$  [16, 32, 192, 384]
- HRN-2x5x2x  $m=16$  [16, 32, 160, 320]

Conclusively, ReLU-equalization only needs prior knowledge of the stagewise criticality of the baseline network, which is often the same for a specific model family, and therefore requires training very few models. Furthermore, ReLU-equalization can be used to design both FLOPs and ReLU efficient neural networks. Thus, going forward, ReLU equalization may offer a new perspective to simplify network design for both FLOPs and ReLU efficient networks and improve interpretability.

## F HybReNet with Different Criticality Order

In this paper, we perform an exhaustive characterization of HRN networks designed for the prevalent criticality order: Stage3 > Stage2 > Stage4 > Stage1. However, we have observed that the criticality order of Stage2 and Stage4 can change in certain cases, such as when using HRNs with  $\alpha=2$  designed for Stage3 > Stage2 > Stage4 > Stage1 criticality order, or when using ResNet18/ResNet34 on TinyImageNet [17]. In these cases, the criticality order changes to Stage3 > Stage4 > Stage2 > Stage1. This leads to the question of whether it is necessary to run the criticality test for every baseline network on different datasets. To answer this, we need to compare the ReLU-accuracy performance of HRN networks designed with the two different criticality orders. To accomplish this, we use the DeepReShape algorithm 1 to design HybReNets for the given criticality order of Stage3 > Stage4 > Stage2 > Stage1.

$$\#ReLUs(S_3) > \#ReLUs(S_4) > \#ReLUs(S_2) > \#ReLUs(S_1) \\ \implies \phi_3\left(\frac{\alpha\beta}{16}\right) > \phi_4\left(\frac{\alpha\beta\gamma}{64}\right) > \phi_2\left(\frac{\alpha}{4}\right) > \phi_1$$

ReLU equalization through width ( $\phi_1 = \phi_2 = \phi_3 = \phi_4 = 2$ , and  $\alpha \geq 2, \beta \geq 2, \gamma \geq 2$ ):

$$\implies \frac{\alpha\beta}{16} > \frac{\alpha\beta\gamma}{64} > \frac{\alpha}{4} > 1 \implies \alpha\beta > 16, \alpha > 4, \alpha\beta\gamma > 64, \beta > 4, \beta\gamma > 16, \text{ and } \gamma < 4$$

Solving the above compound inequalities provides the following range of  $\beta$  and  $\gamma$  at two different  $\gamma$

At  $\gamma = 2$ ,  $\beta > 8$  &  $\alpha > 4$ ; and at  $\gamma = 3$ ,  $\beta > 5$  &  $\alpha > 4$

HRNs with minimum values of  $\alpha$ ,  $\beta$ , and  $\gamma$  satisfying the above ReLU equalization for the altered criticality order: Stage3 > Stage4 > Stage2 > Stage1 are HRN-5x6x3x and HRN-5x9x2x. Further, for lower ReLU counts HRN networks with  $\alpha=2$ , specifically HRN-2x6x3x and HRN-2x9x2x, are chosen. Now, we compare the ReLU-accuracy tradeoffs of these HRNs with those of HRNs designed for the prevalent criticality order, and we used both coarse-grained ReLU optimization (DeepReDuce) and fine-grained ReLU optimization (SNL). The results, depicted in Figure 20, demonstrate that the performance of HRNs for both criticality orders is similar with the coarse-grained optimization on CIFAR-100. However, with fine-grained optimization, we observed a noticeable accuracy gap. Specifically, HRN-2x5x3x and HRN-2x7x2x outperform HRN-2x6x3x and HRN-2x9x2x by a small but discernible margin. Additionally, we compared the performance of HRN-5x6x3x and HRN-5x9x2x on TinyImageNet and found that they performed similarly, except that HRN-5x5x3x outperformed them by a noticeable margin at some intermediate ReLU counts.

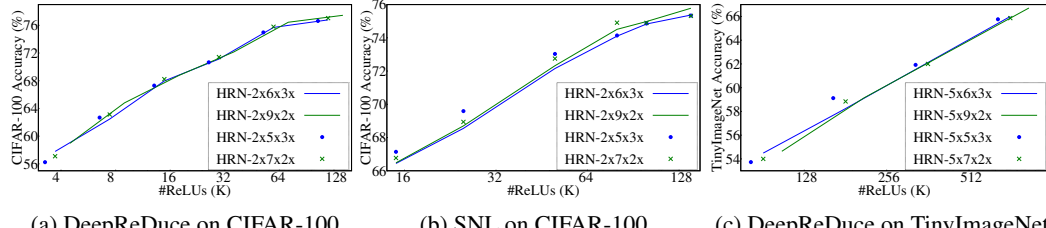


Figure 20: Performance comparison of HRN networks designed for altered criticality order (Stage3 > Stage4 > Stage2 > Stage1), HRNs with  $\beta=6$  and 9, with the HRNs designed for prevalent criticality order (Stage3 > Stage2 > Stage4 > Stage1), HRNs with  $\beta=5$  and 7. Overall, the latter exhibit a slightly better performance than the former.

## G Experimental Results and Discussion for ReLU-reuse

### G.1 Ablation Study on ResNet18

We conducted an ablation study on ResNet18 (CIFAR-100) to investigate the benefits of two techniques: (1) using a shortcut connection between the output of one feature-subspace and the input of the next feature-subspace (shown in Figure 9), and (2) utilizing a fixed number of divisions, independent of the ReLU reduction factor. To evaluate the impact of these techniques, we applied ReLU-reuse on alternate convolution layers of ResNet18 and measured the resulting accuracy, which is reported in Table 14. Our findings suggest that the use of shortcut connections (i.e. with Reuse) leads to improved accuracy, particularly at lower ReLU reduction factors. However, as the ReLU reduction factor increases, the accuracy gain diminishes. For instance, both with and without shortcut connections, we observed a drop of  $\approx 1.5\%$  in accuracy when moving from  $2\times$  to  $4\times$  reduction.

On the other hand, when using a fixed number of divisions in the proposed ReLU-reuse, accuracy drops remains (relatively) stable at higher reduction factors, underscoring the significance of fixed number of divisions and also highlighting their scalability for achieving higher ReLU reduction.

Table 14: We conduct an ablation analysis for ReLU-reuse by integrating it into alternating convolutional layers in ResNet18(CIFAR-100 dataset). For  $N$  partitions, “reuse” signifies a shortcut connection between the output of one feature-subspace and the input of the subsequent one. In our proposed ReLU-reuse, the number of divisions remains constant regardless of the ReLU reduction factor, *offering scalability for greater ReLU reduction factors*.

ReLU reduction factor	ReLU count	N divisions		Proposed
		w/o Reuse	w/ Reuse	(3 divisions)
2x reduction (Scale=2)	434.18K	77.61%	78.19%	77.83%
4x reduction (Scale=4)	372.74K	75.84%	76.87%	77.60%
8x reduction (Scale=8)	342.02K	75.43%	75.66%	76.93%
16x reduction (Scale=16)	326.66K	75.33%	75.47%	76.38%

Nonetheless, we notice that, the proposed ReLU-reuse technique has lower accuracy at scale=2 compared to the  $N$  division with shortcut connections. This is due to the fact that the latter consists of only two groups of feature maps, while the former has three, which resulted in more information loss.

## G.2 Performance Comparison of HRN vs Classical Networks for ReLU-reuse

We conduct a comparative analysis of ReLU-reuse against the conventional scaling method (channel/feature-map scaling) used in DeepReduce [17], on both classical networks and HRNs. To begin with, we employ ReLU-reuse to all the convolutional layers of the networks and reduce the ReLUs by a factor of  $N \in \{2, 4, 8, 16\}$ . For  $N = 2$ , we use the naive ReLU reduction method, as it outperforms the proposed ReLU-reuse (see Figure 9). Our findings reveal that for ResNet18 BaseCh networks, the performance of ReLU-reuse is suboptimal compared to conventional scaling methods, and this performance gap increases for the networks with higher  $m$ . In contrast, on the HRN networks, ReLU-reuse surpasses conventional scaling at higher ReLU reduction factors (at very low ReLU counts). However, at higher ReLUs, particularly for the ReLU reduction factor of two, the information loss resulting from the division of feature maps outweighs the benefits of ReLU-reuse, which lead to inferior performance of ReLU-reuse. We emphasize that this observation holds even for networks with partial ReLU-equalization, such as ResNet18( $m=16$ )-4x4x4x.

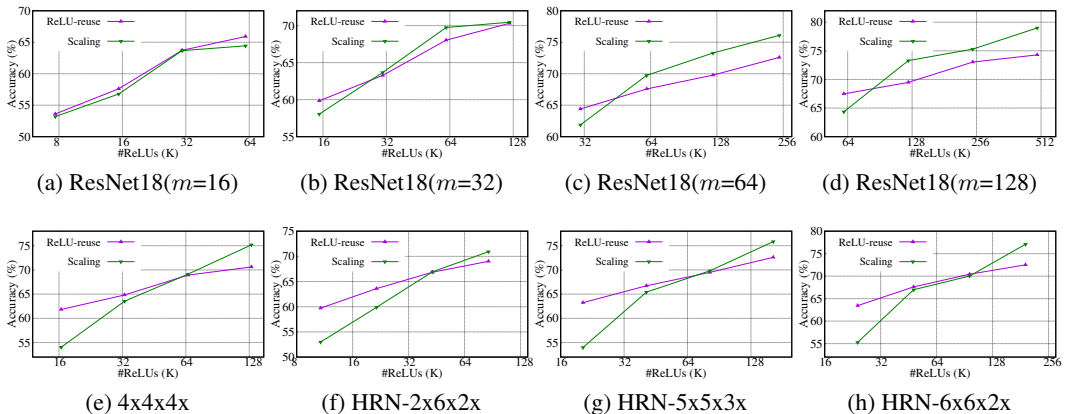


Figure 21: Performance comparison (CIFAR-100) of ReLU-reuse vs conventional scaling (used as reshaping steps in DeepReduce [17]) when ReLU-reuse is employed after every convolution layer.

Furthermore, we conduct the same experiments on Thinned networks, as (channel/feature-map) scaling is performed on Thinned networks in DeepReduce [17]. We dropped ReLUs from alternate convolutional layers and applied ReLU-reuse in the remaining layers. The results are shown in Figure 22. Since ReLU-reuse is now only employed in half of the total number of layers, the cumulative information loss caused by the loss of cross-channel information in feature-map divisions is reduced. As a result, the performance of ReLU-reuse is further enhanced. This improvement is evident from

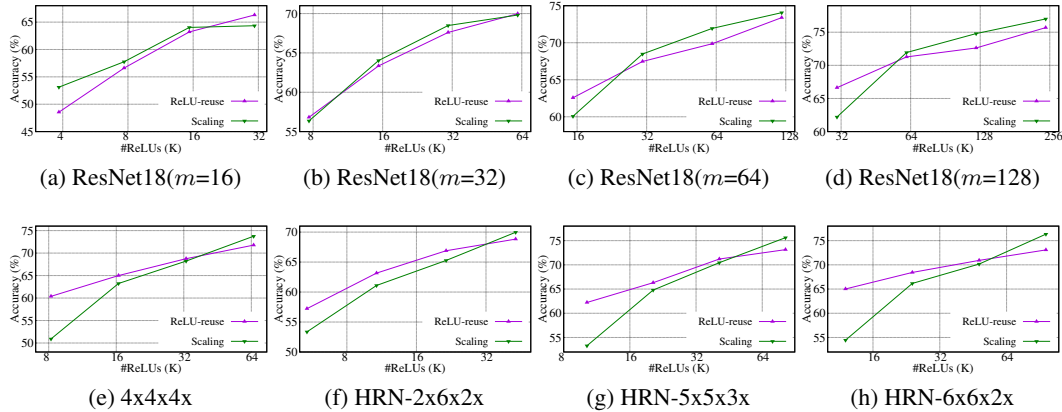


Figure 22: Performance comparison (CIFAR-100) of ReLU-reuse vs conventional scaling (used as reshaping steps in DeepReDuce [17]) when ReLU-reuse is employed in Thinned networks. That is, first ReLU is dropped from every-alternate layers, and then ReLU-reuse is applied in remaining layers.

the change in the performance gap between ReLU-reuse and conventional scaling for all the networks, as shown in Figure 22.

To summarize, the effectiveness of ReLU-reuse depends on the network architecture and the ReLU reduction factor used. Specifically, ReLU-reuse is effective for the networks with (partial/full) ReLU equalization, in contrast with the classical networks, and scales well with higher ReLU reduction factors. Conclusively, *ReLU-Thinned HRN networks combined with ReLU-reuse significantly improve the performance at very low ReLU counts*, and should be further explored in future research.

### G.3 Incorporating ReLU-reuse in ReLU Optimization Pipeline

To improve the performance at extremely low ReLU counts, we incorporate the ReLU-reuse in the ReLU optimization pipeline as outlined in Algorithm 2. Notice that after ReLU-Thinning, we employed conventional channel scaling instead of employing ReLU-reuse (with scaling factor 2), as the latter proved to be inferior due to the cross-channel information loss (see Figures 21 and 22).

Now, we examine the efficacy of ReLU-reuse by employing Algorithm 2 on HRNs with  $\alpha=2$ . For a fair comparison, we adopt the conventional knowledge distillation method [34], as used in prior work[17, 20], instead of decoupled KD (DKD) [35]. As shown in Figure 23, ReLU-reuse consistently outperforms state-of-the-art channel-wise ReLU dropping technique, SNL, by a significant margin across various ReLU counts. In comparison to conventional scaling methods employed in [17], for targeting very low ReLU counts, ReLU-reuse incorporation yields up to a **3%** accuracy boost. This improvement enables HRNs to match the performance of pixel-wise SNL.

## H Design of Experiments and Training Procedure

**Sweeping the width hyperparameters for ReLU-efficiency experiments:** For the network width-based experiments conducted on ResNet models, as illustrated in Figure 3 (a,b), we reduced the base channel count in ResNet18 to  $m=16$  (from  $m=64$ ). This adjustment is required to enable a fair comparison for ResNet models, as the vanilla ResNet20, ResNet32, and ResNet56 have  $\{16, 32, 64\}$  #channels in their successive stages while that in (original) ResNet18 is  $\{64, 128, 256, 512\}$ . For BaseCh networks, we sweep  $m \in \{16, 32, 64, 128, 256\}$  and for StageCh networks we sweep  $(\alpha, \beta, \gamma) = (2, 2, 2)$  to  $(8, 8, 8)$ , homogeneously.

**Training methodology and datasets:** We perform our experiments on CIFAR-100 [57] and Tiny-ImageNet [58, 59] as the prior PI-specific network optimization [17, 20, 21] used these datasets to evaluate their techniques. CIFAR-100 has 100 output classes, each having 500 training and 100

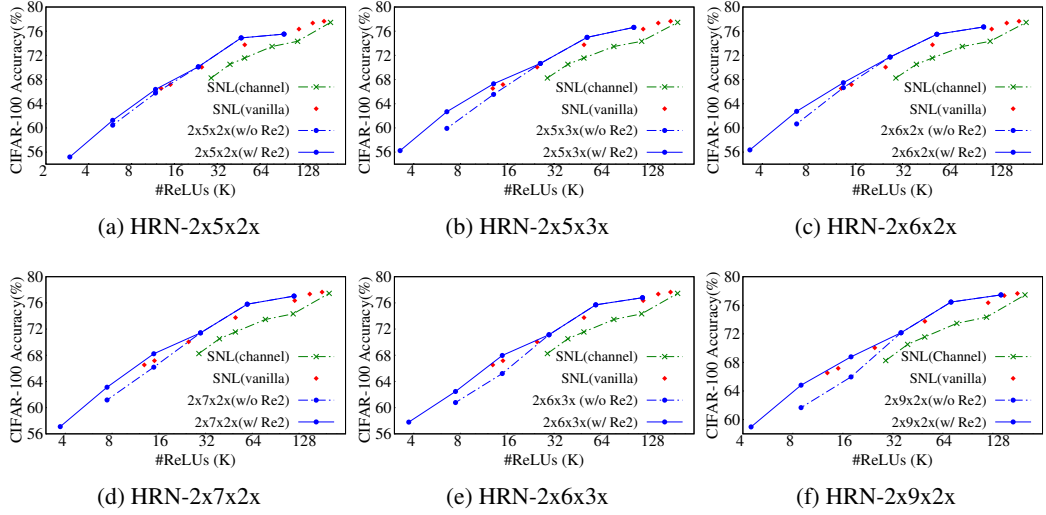


Figure 23: Performance superiority of ReLU-Reuse (Re2) in channel-wise ReLU optimization: Re2 consistently outperforms state-of-the-art channel-wise ReLU dropping technique, SNL, by a significant margin across various ReLU counts. By incorporating Re2, a gain of **1% - 3%** accuracy at iso-ReLU is achieved when compared to the conventional scaling methods (denoted as “w/o Re2”). This gain leads to performance parity with pixel-wise SNL, denoted as “SNL(vanilla).”

---

**Algorithm 2** ReLU optimization for HybReNets(HRNs) using ReLU-reuse

---

**Input:** A network  $Net$  with  $D$  stages  $S_1, S_2, \dots, S_D$  and  $C$ , a sorted list of stages from least to most critical

**Output:** ReLU optimized versions of  $Net$

```

1: if the least critical stage  $C[1]$  has the highest fraction of ReLUs then
2:    $S_k = C[1]$                                  $\triangleright$  Get the least critical stage
3:    $Net = Net - S_k$                           $\triangleright$  Cull the least critical Stage  $S_k$ 
4: end if
5:  $Net_i^T = Thin(Net)$                        $\triangleright$  Thin the remaining stages
6:  $Net_i^C = ScaleCh(Net_i^T, \alpha=0.5)$         $\triangleright$  Channel scaled by 0.5x
7:  $Net_i^{R4} = ReuseReLU(Net_i^T, Sc=4)$         $\triangleright$  ReLU-reuse with scaling factor 4
8:  $Net_i^{R8} = ReuseReLU(Net_i^T, Sc=8)$         $\triangleright$  ReLU-reuse with scaling factor 8
9:  $Net_i^{R16} = ReuseReLU(Net_i^T, Sc=16)$        $\triangleright$  ReLU-reuse with scaling factor 16
10:  $Nets += Net, Net_i^T, Net_i^C, Net_i^{R4}, Net_i^{R8}, Net_i^{R16}$   $\triangleright$  Apply KD to each Net
11: return  $Nets$ 

```

---

test images of resolution  $32 \times 32$ . TinyImageNet, on the other hand, has 200 output classes, each containing 500 training and 50 validation images, each of resolution  $64 \times 64$ .

We train, on both the CIFAR-100 and TinyImageNet datasets, we use cosine annealing learning rate scheduler [60] with an initial learning rate of 0.1, mini-batch size of 128, momentum of 0.9, and 0.0004 weight decay factor. We train networks for 200 epochs on both CIFAR-100 and TinyImageNet; however, we perform 20 additional epochs for warmup when using Decoupled KD [35]. For DeepReDuce experiments, and KD experiments in Tables 5, 11, and 12, we employ Hinton’s knowledge distillation [34] and set the temperature, and relative weight to cross-entropy loss on hard targets as 4 and 0.9, respectively. For SNL, we train the baseline networks using the aforementioned methodology; however, for mask generation, fine-tuning, and knowledge distillation, we used their default implementation. When employing Decoupled knowledge distillation (Tables 5, 11, and 12), we set the relative weight of target class KD as one and vary the weight of non-target class KD as  $\{0.8, 1, 2, 6\}$ . For every experiment involving knowledge distillation, we consistently employed ResNet18 as the teacher model for a fair comparison across the studies.

**Runtime measurement:** We adopt the methodology described in [13] for computing the runtime of a single (private) inference. In particular, we use Microsoft-SEAL for computing the homomorphic encryption (HE) latency, stemming from convolution and fully-connected operations, and DELPHI [9] implementation of Garbled-circuit for computing the garbled-circuit (GC) latency, stemming from ReLU operators. Our experimental setup involves an AMD EPYC 7502 server with specifications of 2.5 GHz, 32 cores, and 256 GB RAM. For these experiments, the client and server are simulated as two separate processes operating on the same machine. To compute the GC latency, we set the number of threads to four. Note that, for HRNs with ReLU-reuse, we computed the HE latency without accounting for the FLOPs reduction, stemming from the group convolution in ReLU-reuse, due to specific implementation constraints of group convolution in Microsoft SEAL.

## I Additional Related Work

**Benefits of width:** The impact of network width on reducing catastrophic forgetting was highlighted by [61]. The influence of network width on the smoothness of the loss surface was analyzed by [62], and found that an increase in width could mitigate erratic behavior in the loss landscape. A study by [63] decoupled the effects of increased width from over-parameterization and find that the width of a network primarily determines its predictive performance, with the number of parameters being a secondary factor, under mild assumptions. [64] established that wider networks, when delivering similar levels of accuracy on the ImageNet dataset, show superior performance on inputs that reflect the scene rather than the objects.

**Challenges and implications of nonlinear layers in diverse neural network applications :** Non-linear layers not only present challenges in private inference but also pose significant obstacles in other domains of neural network application. In optical neural networks, they increase energy and latency overheads due to optical-electrical conversion costs, hindering system efficiency [65, 66]. Adversarial robustness verification becomes complex with ReLU due to unstable neurons [67–69]. Furthermore, the non-distributive nature of ReLU over rotation operations can break the equivariance property of Steerable CNNs [70], known for their parameter and computation efficiency [71–73]; thus, limiting their architectural choices and applicability.

## J Network Architecture of HybReNets

Table 15 shows a comparative analysis of the design hyper-parameters in the conventional WideResNet and ResNet models, with out proposed HybReNets. Table 16 presents a comparison of ResNet18 and WRN22x8, with four HRNs: HRN-5x5x3x, HRN-5x7x2x, HRN-6x6x2x, and HRN-7x5x2x. In comparison to ResNet18, the HRNs allocate fewer channels in the initial stages and more channels in the deeper stages, resulting in a balanced FLOPs-ReLU-accuracy tradeoff. We observed that HRN-5x5x3x offer slightly better FLOPs-ReLU-Accuracy balance compared to other HRNs.

Table 15: Architectural building blocks in (*proposed*) *HybReNet* design for efficient PI. Unlike conventional network widening methods, in ResNet/WideResNet, channels in HybReNet is *heterogeneously* multiplied by a factor of  $\alpha$ ,  $\beta$ , and  $\gamma$  in Stage2, Stage3, and Stage4 (respectively).

Stages	output size	ResNet	WideResNet	HybReNet( <b>Proposed</b> )
Stem	$d_{in} \times d_{in}$	$[3 \times 3, m]$	$[3 \times 3, m]$	$[3 \times 3, m]$
Stage1	$d_{in} \times d_{in}$	$\begin{bmatrix} 3 \times 3, m \\ 3 \times 3, m \end{bmatrix} \times \phi_1$	$\begin{bmatrix} 3 \times 3, m \times k \\ 3 \times 3, m \times k \end{bmatrix} \times \phi_1$	$\begin{bmatrix} 3 \times 3, m \\ 3 \times 3, m \end{bmatrix} \times \phi_1$
Stage2	$\frac{d_{in}}{2} \times \frac{d_{in}}{2}$	$\begin{bmatrix} 3 \times 3, 2m \\ 3 \times 3, 2m \end{bmatrix} \times \phi_2$	$\begin{bmatrix} 3 \times 3, 2m \times k \\ 3 \times 3, 2m \times k \end{bmatrix} \times \phi_2$	$\begin{bmatrix} 3 \times 3, \alpha m \\ 3 \times 3, \alpha m \end{bmatrix} \times \phi_2$
Stage3	$\frac{d_{in}}{4} \times \frac{d_{in}}{4}$	$\begin{bmatrix} 3 \times 3, 4m \\ 3 \times 3, 4m \end{bmatrix} \times \phi_3$	$\begin{bmatrix} 3 \times 3, 4m \times k \\ 3 \times 3, 4m \times k \end{bmatrix} \times \phi_3$	$\begin{bmatrix} 3 \times 3, \beta(\alpha m) \\ 3 \times 3, \beta(\alpha m) \end{bmatrix} \times \phi_3$
Stage4	$\frac{d_{in}}{8} \times \frac{d_{in}}{8}$	$\begin{bmatrix} 3 \times 3, 8m \\ 3 \times 3, 8m \end{bmatrix} \times \phi_4$		$\begin{bmatrix} 3 \times 3, \gamma(\alpha \beta m) \\ 3 \times 3, \gamma(\alpha \beta m) \end{bmatrix} \times \phi_4$
FC	$1 \times 1$	$[\frac{d_{in}}{8} \times \frac{d_{in}}{8}, 8m]$	$[\frac{d_{in}}{8} \times \frac{d_{in}}{8}, 4m \times k]$	$[\frac{d_{in}}{8} \times \frac{d_{in}}{8}, \gamma(\alpha \beta m)]$

Table 16: Comparison of WideResNet22x8 and ResNet18 architecture — predominantly used as input baseline networks in PI-specific ReLU optimization techniques [21, 20, 17] — with our proposed HybReNets (highlighted in **bold**). Unlike the conventional WideResNets and ResNets, the strategic channel allocation in subsequent stages of HybReNets streamline the network’s ReLUs and FLOPs, and simultaneously optimized both the ReLU and FLOPs efficiency. Last rows compare their FLOPs and ReLU counts, along with baseline accuracy (on CIFAR-100).

Stages	output size	WRN22x8	ResNet18	HRN-5x5x3x	HRN-5x7x2x	HRN-6x6x2x	HRN-7x5x2x
Stem	$32 \times 32$	$[3 \times 3, 16]$	$[3 \times 3, 64]$	$[3 \times 3, 16]$	$[3 \times 3, 16]$	$[3 \times 3, 16]$	$[3 \times 3, 16]$
Stage1	$32 \times 32$	$\begin{bmatrix} 3 \times 3, 128 \\ 3 \times 3, 128 \end{bmatrix} \times 3$	$\begin{bmatrix} 3 \times 3, 64 \\ 3 \times 3, 64 \end{bmatrix} \times 2$	$\begin{bmatrix} 3 \times 3, 16 \\ 3 \times 3, 16 \end{bmatrix} \times 2$	$\begin{bmatrix} 3 \times 3, 16 \\ 3 \times 3, 16 \end{bmatrix} \times 2$	$\begin{bmatrix} 3 \times 3, 16 \\ 3 \times 3, 16 \end{bmatrix} \times 2$	$\begin{bmatrix} 3 \times 3, 16 \\ 3 \times 3, 16 \end{bmatrix} \times 2$
Stage2	$16 \times 16$	$\begin{bmatrix} 3 \times 3, 256 \\ 3 \times 3, 256 \end{bmatrix} \times 3$	$\begin{bmatrix} 3 \times 3, 128 \\ 3 \times 3, 128 \end{bmatrix} \times 2$	$\begin{bmatrix} 3 \times 3, 80 \\ 3 \times 3, 80 \end{bmatrix} \times 2$	$\begin{bmatrix} 3 \times 3, 80 \\ 3 \times 3, 80 \end{bmatrix} \times 2$	$\begin{bmatrix} 3 \times 3, 96 \\ 3 \times 3, 96 \end{bmatrix} \times 2$	$\begin{bmatrix} 3 \times 3, 112 \\ 3 \times 3, 112 \end{bmatrix} \times 2$
Stage3	$8 \times 8$	$\begin{bmatrix} 3 \times 3, 512 \\ 3 \times 3, 512 \end{bmatrix} \times 3$	$\begin{bmatrix} 3 \times 3, 256 \\ 3 \times 3, 256 \end{bmatrix} \times 2$	$\begin{bmatrix} 3 \times 3, 400 \\ 3 \times 3, 400 \end{bmatrix} \times 2$	$\begin{bmatrix} 3 \times 3, 560 \\ 3 \times 3, 560 \end{bmatrix} \times 2$	$\begin{bmatrix} 3 \times 3, 576 \\ 3 \times 3, 576 \end{bmatrix} \times 2$	$\begin{bmatrix} 3 \times 3, 560 \\ 3 \times 3, 560 \end{bmatrix} \times 2$
Stage4	$4 \times 4$	$\begin{bmatrix} 3 \times 3, 512 \\ 3 \times 3, 512 \end{bmatrix} \times 2$	$\begin{bmatrix} 3 \times 3, 1200 \\ 3 \times 3, 1200 \end{bmatrix} \times 2$	$\begin{bmatrix} 3 \times 3, 1120 \\ 3 \times 3, 1120 \end{bmatrix} \times 2$	$\begin{bmatrix} 3 \times 3, 1152 \\ 3 \times 3, 1152 \end{bmatrix} \times 2$	$\begin{bmatrix} 3 \times 3, 1120 \\ 3 \times 3, 1120 \end{bmatrix} \times 2$	
FC	$1 \times 1$	$[8 \times 8, 512]$	$[4 \times 4, 512]$	$[4 \times 4, 1200]$	$[4 \times 4, 1120]$	$[4 \times 4, 1152]$	$[4 \times 4, 1120]$
#FLOPs		2461M	559M	1055M	1273M	1368M	1328M
#ReLUs		1393K	557K	343K	379K	401K	412K
Accuracy		81.27%	79.01%	78.40%	78.28%	78.52%	78.81%